

## The Itokawa regolith simulant IRS-1 as an S-type asteroid surface analogue

Xiaojia Zeng<sup>a,c</sup>, Xiongyao Li<sup>a,b,c,\*</sup>, Dayl J.P. Martin<sup>d</sup>, Hong Tang<sup>a,b,c</sup>, Wen Yu<sup>a,b,c</sup>, Kang Yang<sup>e,f</sup>, Zegui Wang<sup>e,f</sup>, Shijie Wang<sup>g</sup>

<sup>a</sup> Center for Lunar and Planetary Sciences, Institute of Geochemistry, Chinese Academy of Sciences, Guiyang 550081, China

<sup>b</sup> CAS Center for Excellence in Comparative Planetology, Hefei, China

<sup>c</sup> Key Laboratory of Space Manufacturing Technology, Chinese Academy of Sciences, Beijing 100094, China

<sup>d</sup> European Space Agency, Fermi Avenue, Harwell Campus, Didcot, Oxfordshire OX11 0FD, United Kingdom

<sup>e</sup> School of Mechanics and Civil Engineering, China University of Mining and Technology, Xuzhou 221116, China

<sup>f</sup> State Key Laboratory for Geomechanics and Deep Underground Engineering, China University of Mining and Technology, Xuzhou 221116, China

<sup>g</sup> State Key Laboratory of Environmental Geochemistry, Institute of Geochemistry, Chinese Academy of Sciences, Guiyang 550081, China

### ARTICLE INFO

#### Keywords:

Asteroid regolith  
IRS-1 simulant  
Surface analogue  
Asteroid exploration

### ABSTRACT

Asteroid regolith simulants (i.e., substitute materials for asteroid surface regoliths) are useful for the preparation of asteroid landing and/or sample-return missions. In this study, we report a new Itokawa asteroid Regolith Simulant (called IRS-1) as an S-type asteroid surface analogue for China's upcoming asteroid exploration. The IRS-1 simulant was developed from mixing terrestrial minerals with appropriate particle size distributions, based on the currently available mineralogy data of S-type asteroid 25143 Itokawa and a LL6 chondrite Sulagiri. Multiple properties of this simulant are well-characterized, including mineralogy, bulk chemistry, particle size, density, mechanical properties, reflectance spectra, thermal properties, thermogravimetry, and hygroscopicity. These results demonstrate that the IRS-1 simulant has similar mineralogy, bulk chemistry, and physical properties to the target materials (i.e., Itokawa samples and LL6 chondrite Sulagiri), making this simulant a reasonable surface analogue of S-type asteroids. Based on the investigation of mechanical properties of the IRS-1 simulant and two other prepared regolith samples (i.e., L-chondrite-like IRS-1L and H-chondrite-like IRS-1H), we found that the mineralogical variations on S-type asteroids have a relatively large influence on the mechanical properties of S-type asteroid regoliths. Our studies show that the IRS-1 simulant will be appropriate for a number of scientific and engineering-based investigations where a large amount (few kilograms to hundreds of kilograms) of sample is required (e.g., technology development, hardware testing, and drilling). This study also provides an effective production approach for the future development of asteroid regolith simulants for different types of asteroid regoliths and associated applications.

### 1. Introduction

During the past decade, China has successfully carried out four lunar exploration missions (i.e., Chang'E-1, Chang'E-2, Chang'E-3, and Chang'E-4), and is preparing to explore Mars in 2020 (e.g., Ouyang et al., 2010; Li et al., 2015; Wei et al., 2018). Following the 'Thirteenth Five-Year Plan' planetary strategy (Wei et al., 2018), China's asteroid exploration mission is also being considered. To reveal the formation and early (~4.5 Ga ago) evolution of the solar system, a sample-return mission from an asteroid (the target is being determined) is expected to launch in the near future (e.g., Zhang et al., 2017; Wei et al., 2018).

Airless asteroids (e.g., Eros and Itokawa) in the Solar System are covered by a layer of unconsolidated geologic material called regolith.

Regolith is formed by continuous impact bombardment and other geologic processes (e.g., space weathering and thermal fatigue) and spans a wide range of particle sizes, from sub-micron to km scales. (Chapman, 1996; Clark et al., 2002; Miyamoto et al., 2007; Delbo et al., 2014). Regolith materials on asteroids preserve the geologic record of planetary evolution, and understanding their physical properties is useful for the engineering design of planetary exploration (e.g., Scheeres et al., 2010; Britt, 2015; Yamada et al., 2016; Matsumoto et al., 2016, 2018; Bierhaus et al., 2018; Thuillet et al., 2018). Asteroid materials that are available for laboratory analysis are mainly from spacecraft sample-return missions (e.g., Hayabusa; Yano et al., 2006; Tsuchiyama et al., 2011) and recovered meteorites (Reddy et al., 2014, 2015). However, asteroid samples are limited for large-scale or

\* Corresponding author at: Center for Lunar and Planetary Sciences, Institute of Geochemistry, Chinese Academy of Sciences, Guiyang 550081, China.  
E-mail address: [lixiongyao@vip.skleg.cn](mailto:lixiongyao@vip.skleg.cn) (X. Li).

destructive scientific and engineering investigations (e.g., engineering-based investigations and drilling studies; Reid et al., 2014; Dreyer et al., 2018; Fries et al., 2018). Thus, a well-characterized asteroid regolith simulant (i.e., the substitute material for asteroid surface regoliths) is needed to ensure the smooth implementation of asteroid exploration (e.g., Seiferlin et al., 2008).

To support asteroid exploration, a series of asteroid regolith simulants have been developed internationally, including HCCL-1 carbonaceous chondrite simulant, UCF/DSI carbonaceous simulants, MPACS comet simulant, and Tagish Lake Simulant (TLS) (Hildebrand et al., 2015; Carey et al., 2017; Bierhaus et al., 2018). Both HCCL-1 and UCF/DSI are general-purpose asteroid regolith simulants based on carbonaceous chondrite meteorites (e.g., CI, CM, and CR; Hildebrand et al., 2015; Covey et al., 2018). The MPACS simulant, developed by NASA's Jet Propulsion Laboratory, was designed to replicate the mechanical properties found in the surface materials of comet nuclei (e.g., low density and high porosity; Carey et al., 2017). Tagish Lake Simulant (TLS) was developed for NASA's first asteroid sample return mission (i.e., Origins, Spectral-Interpretation, Resource-Identification, Security and Regolith-Explorer, OSIRIS-Rex; Bierhaus et al., 2018). This simulant was developed based the properties of the Tagish Lake carbonaceous chondrite meteorite (Hildebrand et al., 2006). In addition, some other terrestrial materials (e.g., lunar soil simulants, sepiolite, meteorites, and silicate glass) have been widely used as asteroid regolith simulants for different applications, including scientific investigations, hardware designs, and technical tests (e.g., Duada et al. 2013; Juaristi et al., 2015; Fries et al., 2018). To date, no well-characterized regolith simulants have been developed to represent S-type asteroid surface regolith.

Due to China's upcoming asteroid exploration missions, demand for an asteroid regolith simulant is increasing. Asteroid 25143 Itokawa is the most fully-characterized S-type asteroid to date (e.g., Miyamoto et al., 2007; Nakamura et al., 2011; Tsuchiyama et al., 2011; Matsumoto et al., 2016), making the Itokawa samples appropriate reference materials from which to develop an S-type asteroid simulant standard. Recently, a new Itokawa asteroid Regolith Simulant (called IRS-1; Fig. 1a) has been developed. Here, we report the raw materials, development processes, and the properties of IRS-1 simulant. The goals of this study are: (1) to provide a reasonable S-type asteroid regolith simulant for scientific and engineering-based applications, and (2) to introduce an effective production approach for other community to develop asteroid simulants. In addition, this work also discusses the effects of mineralogical variation on properties of S-type asteroid regolith and the implications for asteroid regolith simulant development.

## 2. Target regolith simulant

Over 1534 fine regolith particles (i.e.,  $< 114 \mu\text{m}$ ) from the smooth terrain of Itokawa asteroid have been recovered by Hayabusa spacecraft (Tsuchiyama et al., 2011). The mineralogy and properties of S-type asteroid 25143 Itokawa regolith have been applied to the IRS-1 simulant standard. Investigations of the Itokawa regolith samples and associated remote-sensing data have confirmed that the Itokawa materials are mineralogically and geochemically similar to thermally metamorphosed LL4 to LL6 chondrites (e.g., Abe et al., 2006; Nakamura et al., 2011, 2014; Tsuchiyama et al., 2014). We therefore also take the properties (e.g., bulk chemistry and physical properties) of LL-chondrite samples (e.g., the Sulagiri LL6 chondrite meteorite; Weisberg et al., 2009) as reference data for the development of the IRS-1 simulant. Taken together, the following available data for S-type asteroid materials can be used as guidelines for the target simulant.

### 2.1. Mineralogy

The mineralogy of asteroid Itokawa is well understood from analyses of the Hayabusa spacecraft returned samples (Nakamura et al.,

2011; Tsuchiyama et al., 2011; Langenhorst et al., 2014; Keller and Berger, 2014). These materials are mainly composed of olivine (67 wt %), clinopyroxene (18 wt%), orthopyroxene (2 wt%), plagioclase (9 wt %), troilite (3 wt%), metal (0.53 wt%), and trace (0.21 wt%) amounts of chromite and Ca-phosphate (Tsuchiyama et al., 2011). The mineralogical results of the IRS-1 simulant are consistent with the mineralogy for LL-chondrite (Table 1).

### 2.2. Bulk chemistry

Despite the returned Itokawa particles being too few to carry out whole rock composition analysis, its bulk composition can be estimated from the modal mineralogy and mineral chemistry results (Nakamura et al., 2014; Table 2 and Table 3). This calculated composition is generally similar to the average bulk composition of LL-chondrites and the studied Sulagiri LL6 chondrite (see Table 2).

### 2.3. Particle size characteristics

To date, there is still a lack of representative asteroid material to obtain particle size distributions of asteroid regolith, although the fine-grained ( $< 114 \mu\text{m}$ ) Itokawa particles have been characterized (Tsuchiyama et al., 2011; Sánchez and Scheeres, 2014). However, particle size characteristics of asteroid regolith can be estimated from the high-resolution images taken by Hayabusa spacecraft, and also from theoretical studies (e.g., using remote measurements of the thermal inertia; Jewitt et al., 2010; Gundlach and Blum, 2013). The close-up images of Itokawa revealed that the major portion of Itokawa's regolith is most likely millimeter-sized grains (Fig. 1b), rather than powdery particles (e.g., Yano et al., 2006; Miyamoto et al., 2007; Noviello et al., 2014). This observation is consistent with the theoretical estimation (using thermal inertia) that small bodies in solar system (i.e., diameter less than  $\sim 100 \text{ km}$ ) could be covered by regolith with particle sizes in the millimeter to centimeter range (Sánchez and Scheeres, 2014). Considering the sampling size (e.g., may be tens of grams; Zhang et al., 2017) designed for China's asteroid exploration, the fine-grained (i.e., sub-millimeter to millimeter) regoliths will be more reliable for collection compared to the relatively large rock fragments on the asteroid's surface. We therefore aim for the grain size of the target simulant to be  $< 2000 \mu\text{m}$  and the median particle size to be  $\sim 800 \mu\text{m}$ .

### 2.4. Physical and mechanical properties

The average grain density of Itokawa samples is  $3.4 \text{ g/cm}^3$  (Tsuchiyama et al., 2011), which is similar to the measured grain density of LL-chondrites ( $3.54 \pm 0.13 \text{ g/cm}^3$ ; Consolmagno et al., 2008). Additionally, the angle of friction of blocks on the surface of asteroid Itokawa has been estimated to be  $40^\circ$  (Aoki et al., 2014).

## 3. Materials and methods

### 3.1. Raw materials

Minerals are the basic components of surface regoliths on S-type asteroids. We therefore develop the regolith simulant by combining terrestrial minerals according to mineralogical components of Itokawa samples and LL-chondrites (Table 1). The raw silicate phases used for development of IRS-1 simulant include olivine, orthopyroxene, clinopyroxene, and albite (Fig. 1a). Because troilite (FeS) and nickel-iron metal (i.e., kamacite and taenite) are commonly found in meteorites but are rare on the Earth (Rubin and Ma, 2017), we replaced them with widely available pyrrhotite ( $\text{Fe}_{1-x}\text{S}$ ,  $x = 0-0.2$ ) and iron filings (Fig. 1f) respectively in the IRS-1 simulant. Considering only a small proportion ( $< 1.7 \text{ wt\%}$ ) of accessory minerals (e.g., chromite and phosphate) were detected in Itokawa samples and ordinary chondrites (Table 1), these mineral phases were not chosen as raw materials for the development of

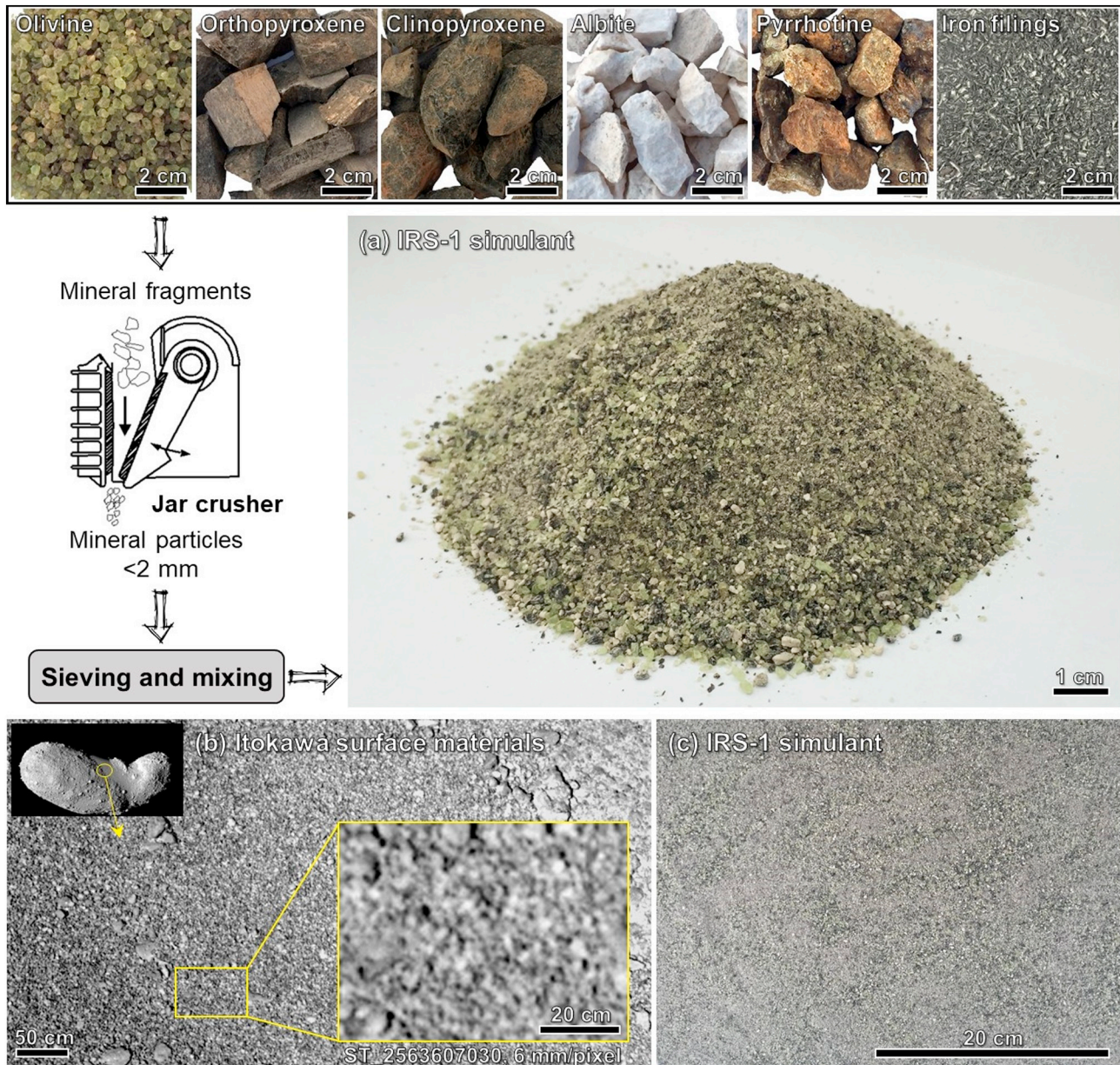


**Fig. 1.** A schematic diagram illustrating the raw materials and production processes of IRS-1. (a) The powder IRS-1 simulant. (b–c) Comparison of Itokawa surface materials with the IRS-1 simulant. The close-up image of ST\_2563607030, with resolution of 0.6 cm/pixel, was taken from 63 m altitude by Hayabusa spacecraft (Yano et al., 2006; Miyamoto et al., 2007).

**Table 1**  
Mineralogy abundance of Itokawa samples, Sulagiri, ordinary chondrites, and IRS-1.

	Simulant reference (wt%)		Ordinary chondrites <sup>c</sup> (wt%)			IRS-1 simulant Replace minerals	wt%
	Itokawa <sup>a</sup>	Sulagiri (LL6) <sup>b</sup>	LL-chondrite	L-chondrite	H-chondrite		
Olivine	67	53.5	51.1 ± 2.2	42.1 ± 1.9	32.8 ± 3.0	Olivine (Fo <sub>91.6</sub> )	60
Orthopyroxene	18	21.0	21.1 ± 2.0	23.3 ± 1.8	25.9 ± 2.2	Orthopyroxene (En <sub>69.3</sub> Wo <sub>1.2</sub> )	20
Clinopyroxene	2	8.2	7.4 ± 0.9	8.0 ± 1.1	6.5 ± 1.3	Clinopyroxene (En <sub>40.5</sub> Wo <sub>44.8</sub> )	5
Plagioclase	9	10.8	9.7 ± 0.8	9.2 ± 1.3	8.7 ± 1.5	Plagioclase (Albite, Ab <sub>95.2</sub> )	10
Troilite	3	3.8	5.7 ± 1.5	7.2 ± 2.0	5.8 ± 0.7	Pyrrhotine	3
Nickel-iron metals	0.53	2.6	3.5 ± 2.0	8.4 ± 0.8	18.6 ± 2.4	Iron filings	2
Others <sup>d</sup>	0.21	< 1	1.6 ± 0.1	1.6 ± 0.2	1.7 ± 0.1	–	–

<sup>a</sup> Tsuchiyama et al., 2011.

<sup>b</sup> Calculated from the modal mineralogy of Sulagiri and the densities of minerals (Tsuchiyama et al., 2011).

<sup>c</sup> Modal abundance of ordinary chondrites (OCs) was taken from Dunn et al. (2010).

<sup>d</sup> Others include chromite, apatite, merrillite, etc. (Dunn et al., 2010; Tsuchiyama et al., 2011).

**Table 2**

Representative EDS data for silicate phases in the IRS-1 simulant, compared with the mineral composition of Itokawa samples and LL 6 chondrite Sulagiri.

Itokawa samples (EMPA) <sup>a</sup>				Sulagiri LL6 chondrite (EDS)				IRS-1 simulant (EDS)			
Ol	Opx	Cpx	Pl	Ol	Opx	Cpx	Pl	Ol	Opx	Cpx	Pl
SiO <sub>2</sub>	38.0 ± 0.49	54.9 ± 0.74	53.9 ± 1.05	65.5 ± 1.10	36.1	53.4	51.7	60.9	39.1	51.0	45.8
TiO <sub>2</sub>	b.d.	0.16 ± 0.02	0.37 ± 0.05	0.04 ± 0.03	0.28	0.28	0.45	0.49	0.11	0.15	1.62
Al <sub>2</sub> O <sub>3</sub>	b.d.	0.16 ± 0.03	0.62 ± 0.55	20.2 ± 0.35	b.d.	0.43	0.79	21.7	0.11	3.39	9.29
Cr <sub>2</sub> O <sub>3</sub>	b.d.	0.09 ± 0.03	0.65 ± 0.08	b.d.	0.28	0.15	0.64	0.32	b.d.	0.08	0.22
FeO	26.2 ± 0.53	15.8 ± 0.37	5.31 ± 0.50	0.37 ± 0.24	22.8	14.5	5.20	0.49	8.42	18.9	8.22
MnO	0.47 ± 0.02	0.46 ± 0.02	0.23 ± 0.02	0.03 ± 0.02	0.36	0.44	0.25	0.20	0.09	0.23	0.31
MgO	36.0 ± 0.53	27.6 ± 0.42	16.2 ± 0.52	0.14 ± 0.20	39.6	29.6	16.8	0.63	51.5	24.9	12.7
CaO	b.d.	0.70 ± 0.15	21.6 ± 0.62	2.18 ± 0.10	0.19	0.73	23.2	2.22	0.16	0.60	19.5
Na <sub>2</sub> O	b.d.	0.02 ± 0.01	0.56 ± 0.16	9.63 ± 0.45	0.11	0.25	0.85	11.9	0.33	0.57	2.04
K <sub>2</sub> O	b.d.	0.03 ± 0.04	0.95 ± 0.21	0.15	0.12	b.d.	1.04	0.07	b.d.	0.27	0.19
P <sub>2</sub> O <sub>5</sub>	0.05 ± 0.03	b.d.	b.d.	0.05 ± 0.03	b.d.	0.13	b.d.	0.16	0.08	0.10	b.d.
Total	100.6	99.83	99.44	99.14	100.0	100.0	100.0	100.0	100.0	100.0	100.0
Fo	71.0				75.6				91.6		
En		74.7	46.6		77.4	46.3			69.3	40.5	
Wo		1.4	44.8		1.4	45.7			1.2	44.8	
Ab				84.0				86.1			95.2

b.d. = below the detection limit.

<sup>a</sup> Average composition and one sigma variations of Itokawa highly equilibrated particles (Nakamura et al., 2011).**Table 3**

Bulk major-element chemistry of IRS-1, compared with the bulk composition of Itokawa samples, LL 6 chondrite Sulagiri, and LL-chondrite meteorites (wt%).

	Itokawa samples <sup>a</sup> (Nakamura et al., 2014, 2SD)	Itokawa samples <sup>a</sup> (Nakamura et al., 2011)	LL-chondrite <sup>b</sup> (average, 2SD)	LL6 chondrite Sulagiri	IRS-1 simulant (N = 3, 2SD)
SiO <sub>2</sub>	42.4 ± 5.68	42.5	40.6 ± 1.08	39.9	42.7 ± 0.06
TiO <sub>2</sub>	0.05 ± 0.02	0.05	0.13 ± 0.04	0.32	0.44 ± 0.05
Al <sub>2</sub> O <sub>3</sub>	1.77 ± 0.36	1.80	2.24 ± 0.16	2.29	3.40 ± 0.05
Cr <sub>2</sub> O <sub>3</sub>	0.11 ± 0.04	0.11	0.54 ± 0.06	0.59	0.05
FeO/Fe <sub>2</sub> O <sub>3</sub> <sup>c</sup>	23.3 ± 3.76	23.4	28.1 ± 4.12	30.3	15.8 ± 0.10
MnO	0.41 ± 0.06	0.40	0.35 ± 0.04	0.36	0.16
MgO	29.6 ± 5.12	29.5	25.2 ± 0.88	25.2	34.3 ± 0.08
CaO	0.90 ± 0.32	0.86	1.92 ± 0.22	1.92	1.47
Na <sub>2</sub> O	0.84 ± 0.18	0.85	0.95 ± 0.12	0.95	1.06 ± 0.02
K <sub>2</sub> O	0.08 ± 0.04	0.08	0.10 ± 0.04	0.10	0.04
P <sub>2</sub> O <sub>5</sub>	0.06 ± 0.04	0.04	0.22 ± 0.08	0.23	0.05
Total	99.5	99.5	100.3	102.2	99.4
FeO/Fe <sub>2</sub> O <sub>3</sub> + MgO	52.9	52.9	53.3	55.5	50.1

<sup>a</sup> The bulk composition is determined by modal reconstruction (Nakamura et al., 2011, 2014).<sup>b</sup> The average bulk composition of LL-chondrite meteorites was taken from Jarosewich (1990).<sup>c</sup> The total iron for Itokawa samples expressed as FeO, while the total iron for LL-chondrite, Sulagiri LL6 chondrite, and IRS-1 simulant expressed as Fe<sub>2</sub>O<sub>3</sub>.

### IRS-1 simulant

Most of minerals used for the development of IRS-1 are sourced from mines in China. The pyroxene (orthopyroxene and clinopyroxene), albite, and pyrrhotite minerals are from Xinjiang province, Hubei province, and Hebei province, respectively. The olivine grains are sourced from the peridotite xenolith in Hebei province, China. These raw materials are available commercially and easily acquired at low cost, making the IRS-1 simulant reproducible in large quantities and readily accessible by the community.

### 3.2. Preparation of IRS-1 simulant

The IRS-1 simulant was prepared via the following steps: (1) Raw material crushing. Using the jaw crusher, the coarse-grained (i.e., 0.5–5 cm in diameter) raw mineral fragments were crushed into fine-grained particles (i.e., < 0.5 mm in diameter). A jaw crusher was chosen because the main process for breaking down material on airless bodies is also mechanical (due to meteorite impacts; e.g., Miyamoto et al., 2007). (2) Sieving and particle size adjustment. Each of the crushed minerals was sieved and then adjusted for size distribution, according to the designed particle characters (i.e., < 2000 µm, D90 = 1400 µm, D50 = 800 µm, and D10 = 100 µm). (3) Mixing the mineral components. The sieved mineral powders were mixed in the

proportions listed in Table 1. Specifically, these mineral components are 60 wt% olivine, 20 wt% orthopyroxene, 5 wt% clinopyroxene, 10 wt % plagioclase, 3 wt% pyrrhotite, and 2 wt% iron filings (Table 1). In the production process, these procedures described above have been documented in detail to ensure that the IRS-1 simulant can be re-produced in the future.

Ordinary chondrite meteorites (LL-chondrite, L-chondrite, and H-chondrite) are thought to be similar to materials on S-type asteroids (Rivkin, 2013). The prepared IRS-1 simulant is mineralogically similar to LL-ordinary chondrites (Table 1), while the mineralogy of this simulant is different from that of other ordinary chondrite sub-groups, i.e., L-chondrite and H-chondrite (Table 1). In order to investigate how mineral variations will have an effect on physical properties of the simulant, L-chondrite-like (IRS-1L) and H-chondrite-like (IRS-1H) samples have also been prepared, following the development method of IRS-1 simulant. The mineralogy (wt%) of IRS-1L (40% olivine, 24% orthopyroxene, 8% clinopyroxene, 10% albite, 8% pyrrhotine, and 10% iron filings) is similar to that of L-chondrite meteorites (Table 1). In contrast, the mineralogy (wt%) of IRS-1H (30% olivine, 25% orthopyroxene, 8% clinopyroxene, 9% albite, 8% pyrrhotine, and 20% iron filings) is similar to that of H-chondrite meteorites (Table 1). Both IRS-1L and IRS-1H have similar particle size distributions as the IRS-1 simulant.



**Fig. 2.** (a) Hand sample of LL6 chondrite meteorite Sulagiri, weighing ~17 g; (b) BSE image of the representative area of Sulagiri, showing this meteorite is mainly composed of olivine (Ol), orthopyroxene (Opx), clinopyroxene (Cpx), plagioclase (Pl), troilite (Tro), and Fe-Ni metal (Fe-Ni).

### 3.3. Analytical methods

The IRS-1 simulant is being produced at the Institute of Geochemistry, Chinese Academy of Sciences. Initially, several polished thick sections and powdered (< 50 μm) samples of this simulant were prepared and studied using a variety of analytical techniques. Also, we acquired a ~17 g sample of the LL6 ordinary chondrite meteorite, officially named Sulagiri from a fall in 2008 in India (Fig. 2; Weisberg et al., 2009), for investigating the mineralogy, bulk chemistry, reflectance spectra, and thermogravimetry properties for comparison with the IRS-1 simulant.

Back-scattered electron (BSE) images were collected using a FEI Scios dual-beam focused ion beam/scanning electron microscope (FIB/SEM) at the Institute of Geochemistry, Chinese Academy of Sciences. The operating conditions were 15–20 kV accelerating voltage, 1.6–3.2 nA beam current, and 7–8 mm working distance. The mineral composition was studied using the same FEI Scios FIB/SEM and an energy dispersive spectrometer system (EDS, manufactured by EDAX), with the same current and voltage settings as noted above. Modal abundances of minerals in the section of Sulagiri chondrite were estimated by combining BSE images with the EDS data (e.g., Zeng et al., 2018). Additionally, SEM images of the IRS-1 simulant were used to identify particle shapes and to calculate the particle aspect ratios with image analysis Nano measurer software. Here, the aspect ratio, AR, of a particle is defined as the ratio of its length to width.

X-ray diffraction (XRD) patterns of IRS-1 simulant and Sulagiri chondrite were collected on a Panalytical multifunction X-ray diffractometer (Empyrean) at the Institute of Geochemistry, Chinese Academy of Sciences. The data was collected in the 2θ range of 4–60°, with a step size of 0.013° and a counting time of 5 s per step (Meng et al., 2016).

Bulk-rock major element compositions of IRS-1 and Sulagiri LL6

chondrite were determined by X-ray fluorescence spectrometry (ARL Perform'X Sequential XRF) at the Institute of Geochemistry, Chinese Academy of Sciences, following standard procedures (e.g., Deng et al., 2017). The accuracy and precision of the XRF analyses are estimated to be ~2% for major oxides present in concentrations > 0.5 wt%.

Mechanical properties (i.e., cohesion and angle of friction) of IRS-1 simulant and another two IRS-1 based samples (i.e., L-chondrite-like IRS-1L and the H-chondrite-like IRS-1H) were determined by consolidated drained (CD) triaxial tests at the China University of Mining and Technology, with loading rates of 0.05 mm/s and confining pressures of 50, 100, and 150 kPa. The standard procedures for specimen preparation and the triaxial test were based on the Chinese standard GB/T50123-1999 (Li et al., 2018). All of these samples were analyzed at the same conditions.

We measured the reflectance spectra of IRS-1 simulant and Sulagiri LL6 chondrite using an Agilent Cary 5000 Ultraviolet-Visible-Near-Infrared (UV-Vis-NIR) spectrophotometer at the Institute of Geochemistry, Chinese Academy of Sciences. These two samples were dried at ~100 °C overnight before conducting the test. The spectra were acquired in the wavelength range of 400–2500 nm at room temperature and normal atmospheric pressure.

Thermal properties of the IRS-1 simulant were measured by Hot Disk TPS 2500S Thermal Constants Analyzer using the transient plane source technique (the test was repeated three times) at Institute of Geochemistry, Chinese Academy of Sciences. The uncertainty for this measurement is estimated at ~3%. A stainless steel sheet was used as a testing standard (Yu et al., 2016). All measurements were conducted at room temperature (~25 °C) and normal atmospheric pressure.

Thermal stability characterization of IRS-1 simulant and Sulagiri chondrite were analyzed by using a Thermogravimetric Analysis (TGA) technique (STA-449C, Netzsch Instruments, Germany). Each oven-dried sample (~20 mg) was heated from 50 °C to 1000 °C at a heating rate of 20 °C/min. Analyses were done under atmospheric pressure (Qin et al., 2017).

## 4. Characteristics of the IRS-1 simulant

### 4.1. Mineralogy

The mineralogy of IRS-1 simulant was characterized to compare with the LL6 chondrite Sulagiri by using XRD, SEM, and EDS techniques (Figs. 3 and 4). The XRD pattern for IRS-1 simulant is broadly consistent with the XRD pattern for LL6 chondrite Sulagiri (Fig. 3). Both of them are dominated by peaks associated with olivine, orthopyroxene, clinopyroxene, and albite. These silicate phases were easily recognized in the scanned image, where the green, dark gray, and white grains

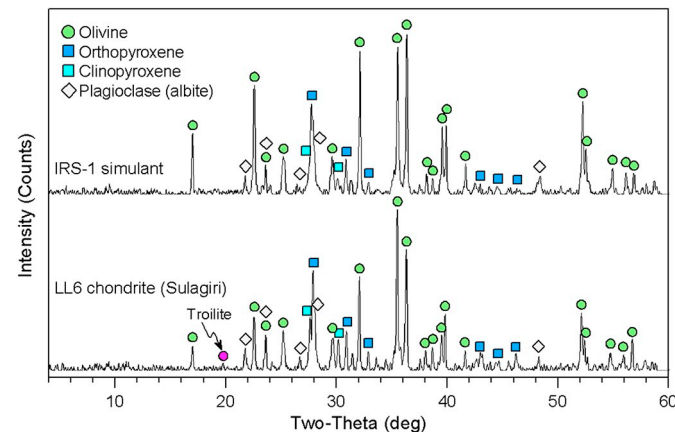


**Fig. 3.** X-ray diffraction patterns for IRS-1 and Sulagiri LL6 chondrite, showing that both samples are mainly composed of olivine, orthopyroxene, clinopyroxene, and plagioclase.

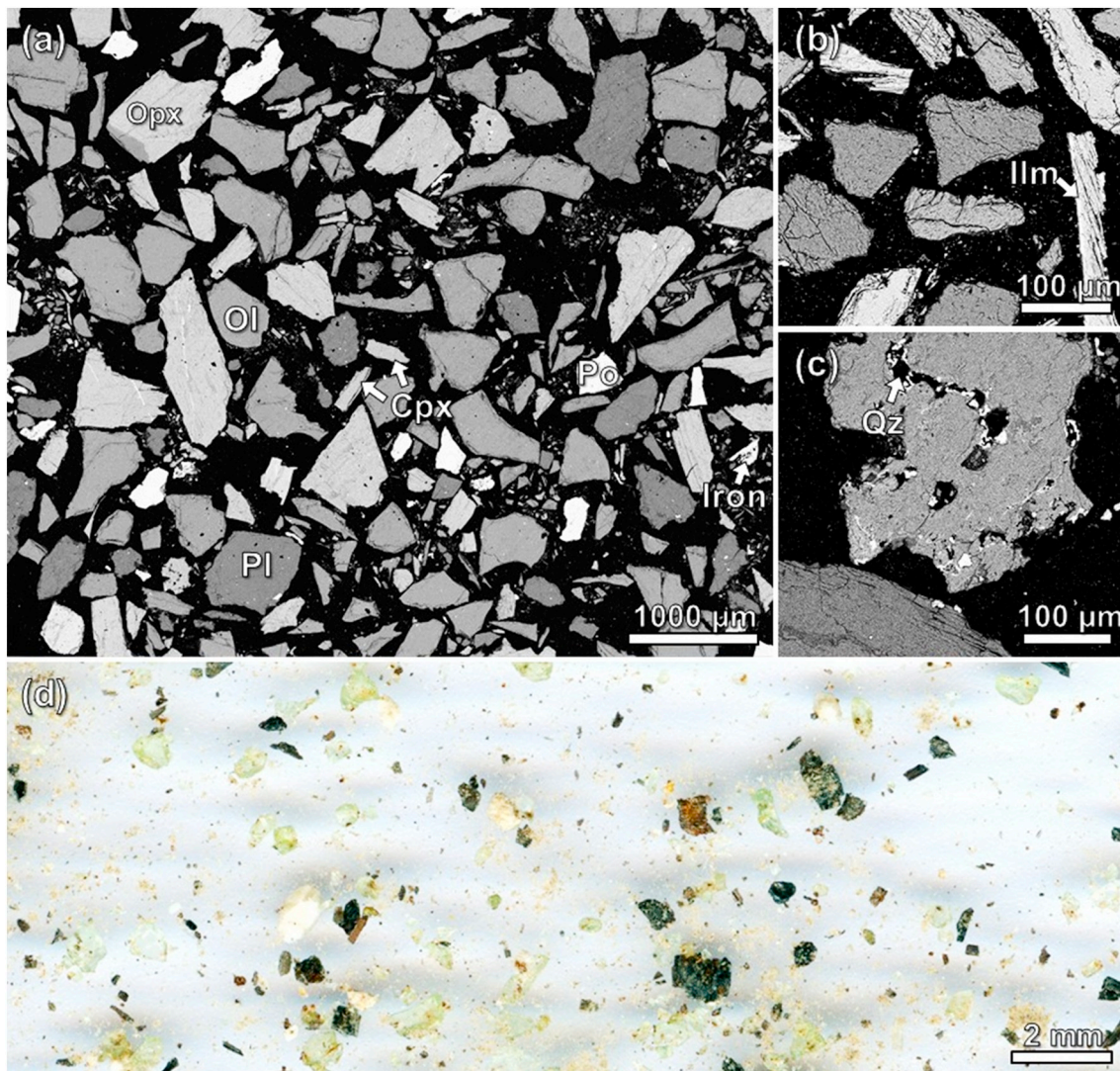


**Fig. 4.** BSE (a–c) and scanned (d) images of IRS-1 simulant, showing the mineralogy and particle shapes of this simulant. The mineral phases are labeled: Ol = olivine; Opx = orthopyroxene; Cpx = clinopyroxene; Pl = plagioclase; Po = pyrrhotite; Iron = iron filing; Ilm = ilmenite; Qz = quartz (Whitney and Evans, 2010).

represent olivine, pyroxene, and plagioclase grains, respectively (Fig. 4d). In addition, trace amounts of troilite grains have been detected in the XRD pattern of Sulagiri chondrite. Due to the raw minerals for producing IRS-1 simulant being obtained from natural rocks, it should be noted that there are minor impurities (< 1 wt% of e.g., ilmenite and quartz) that have been detected from the SEM-EDS analysis (Fig. 4b–c).

For individual silicate minerals in IRS-1 simulant, the EDS data suggests that olivine, orthopyroxene, clinopyroxene, and plagioclase in this simulant tend to be forsteritic olivine ( $\text{Fo}_{91.6}$ ), pigeonite ( $\text{En}_{69.3}\text{Wo}_{1.2}$ ), augite ( $\text{En}_{40.5}\text{Wo}_{44.8}$ ), and albite ( $\text{Ab}_{95.2}$ ), respectively (Table 2). The mineral composition for pyroxene is generally similar to that in Itokawa samples and Sulagiri chondrite, whilst olivine grains ( $\text{Fo}_{91.6}$ ) in IRS-1 simulant are relatively magnesium-rich compared with olivine grains ( $\text{Fo}_{71-75}$ ) in Itokawa samples and Sulagira chondrite (Table 2).

#### 4.2. Bulk chemistry

Bulk major element compositions of LL6 chondrite Sulagiri and three IRS-1 simulants were measured using an XRF technique (Table 3). The bulk chemistry of Sulagiri LL6 chondrite is generally within the

range of the reported average bulk composition of LL-chondrite meteorites (Jarosewich, 1990). For IRS-1 simulant, it has relatively high abundance of  $\text{SiO}_2$  (42.7 wt%),  $\text{Al}_2\text{O}_3$  (3.40 wt%),  $\text{Fe}_2\text{O}_3$  (15.8 wt%),  $\text{MgO}$  (34.3 wt%), and  $\text{CaO}$  (1.47 wt%), with relatively low contents of  $\text{TiO}_2$  (0.44 wt%),  $\text{MnO}$  (0.16 wt%), and  $\text{NaO}$  (1.06 wt%). These element compositions are broadly similar to the calculated bulk composition of Itokawa samples and LL6 chondrite Sulagiri, except for  $\text{Al}_2\text{O}_3$ ,  $\text{FeO}/\text{Fe}_2\text{O}_3$ , and  $\text{MgO}$  contents (see Table 3).

#### 4.3. Particle shape and size distribution

Particle shape and size characteristics are some of the dominant factors that affect the physical and mechanical properties of a regolith simulant. From the BSE and scanning images (Fig. 4a and d), it is clear that the IRS-1 simulant shows a wide range of particle shapes, ranging from sub-rounded to extremely angular, which is generally similar to the particle shapes of Itokawa returned samples (e.g., Fig. 1 of Tsuchiyama et al., 2011; Fig. 3 of Nakamura et al., 2011). The aspect ratio of IRS-1 simulant is predominantly around 1–3, with an average value of 1.98 ( $N = 562$ ) (see Fig. 5). Fig. 6 presents the particle size distribution of IRS-1 simulant, showing that the particles in IRS-1 simulant are < 2000  $\mu\text{m}$  in diameter. The D90, D50, and D10 of this

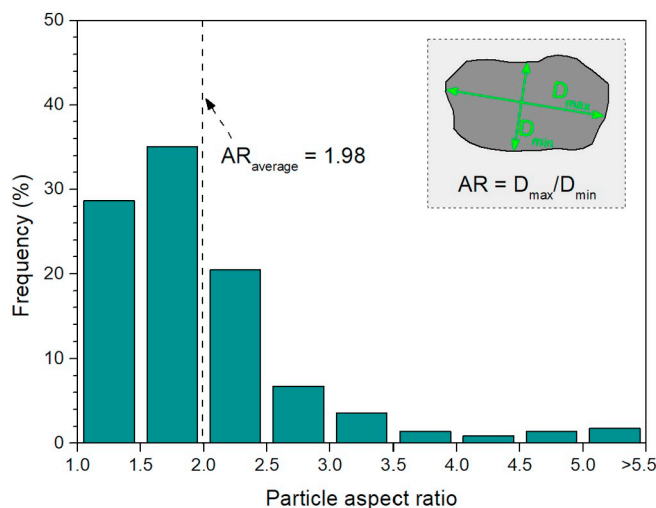


**Fig. 5.** Particle aspect ratio (AR) distribution obtained using scanning electron microscopy (SEM) analysis for the IRS-1 simulant. The aspect ratio of 562 particles were counted.

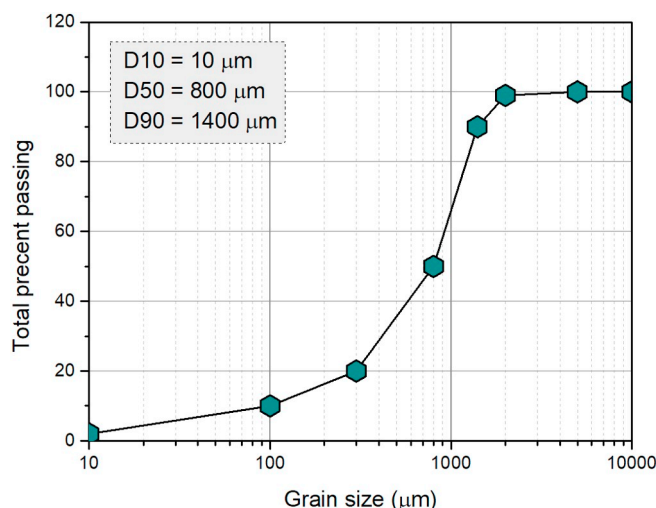


**Fig. 6.** Particle size distribution of IRS-1 simulant, showing this simulant has grain size  $< 2000 \mu\text{m}$ , with the median size of  $800 \mu\text{m}$ .

simulant are  $1400 \mu\text{m}$ ,  $800 \mu\text{m}$ , and  $100 \mu\text{m}$ , respectively.

#### 4.4. Specific gravity and bulk density

The specific gravity refers to the ratio of particle mass to the mass of an equal volume of water at  $4^\circ\text{C}$ . The measured average specific gravity for IRS-1 simulant is  $3.37 \pm 0.27 \text{ g/cm}^3$  ( $N = 3$ , 2SD). To determine the bulk density of IRS-1 simulant, the mass and volume of three simulants were measured, resulting in an average bulk density of  $1.62 \pm 0.03 \text{ g/cm}^3$  ( $N = 3$ , 2SD). These specific gravity and bulk density values are critical parameters when using geological materials for mechanical testing, such as sample collection tests (Bierhaus et al., 2018).

#### 4.5. Mechanical properties

Mechanical properties (e.g., cohesion and angle of friction) are important parameters when regolith simulants are used for engineering applications (e.g., Bierhaus et al., 2018). Measurements of IRS-1 simulant show that this simulant has cohesion and angle of friction values of 10.02 and 46.8, respectively (Table 4). To evaluate the effects of

mineralogical variations on mechanical properties of S-type regolith, we also prepared two more samples for mechanical investigation (i.e., the L-chondrite-like IRS-1L and the H-chondrite-like IRS-1H; Table 4) based on the mineralogy of L and H ordinary chondrites (Table 1). These two samples have similar particle size distributions as the IRS-1 simulant, and their mechanical properties have been determined by the same analytical conditions for IRS-1 measurements. The results indicate that the three analyzed samples (i.e., Itokawa/LL-chondrite-like IRS-1, L-chondrite-like IRS-1L, and H-chondrite-like IRS-1H) have different angles of friction (i.e., 46.8 for IRS-1, 42.2 for IRS-1L, and 47.3 for IRS-1H; Fig. 7).

#### 4.6. Reflectance spectra

Fig. 8 presents the reflectance spectrum of the IRS-1 simulant in the visible to near-infrared range (i.e., 400–2500 nm), compared with the spectrum of LL6 chondrite Sulagiri. The spectra of asteroid 2514 Itokawa, an S-type asteroid, and ordinary chondrite meteorite were also plotted for comparison. As shown in Fig. 8, the measured spectrum of IRS-1 simulant is broadly similar to the spectrum for LL6 chondrite Sulagiri. Both samples have two strong absorption bands at  $\sim 900$ – $1000$  nm and  $\sim 1900$  nm. Fig. 9 shows the continuum removed spectra of these two samples. The  $\sim 900$ – $1000$  nm mineral absorption band is the result of the presence of either pyroxene or olivine or both, while the  $\sim 1900$  nm band is indicative of the presence of pyroxene (Binzel et al., 2001). Weak absorption bands at  $\sim 1400$  nm are related to the OH<sup>-</sup> stretching associated with structurally bound OH and H<sub>2</sub>O, while the  $\sim 2200$  nm and  $\sim 2300$  nm absorptions may be due to metal-OH (e.g., Al-OH and Fe,Mg-OH) transitions (Clark, 1999). Absorptions at  $\sim 1250$  nm are caused by plagioclase in both the IRS-1 simulant and LL6 chondrite Sulagiri (Anbazhagan and Arivazhagan, 2009). Also, absorption from Fe<sup>3+</sup> are presented at  $\sim 500$  nm and  $\sim 650$  nm in both samples (Anbazhagan and Arivazhagan, 2009).

#### 4.7. Thermal properties

Thermal properties of terrestrially made simulants are of great importance to developing methods of extraterrestrial resource utilization, and for estimating the physical properties of planetary materials (e.g., Street Jr et al., 2010; Siegler et al., 2012; Sakatani et al., 2018). At ambient conditions (i.e. room temperature,  $\sim 25^\circ\text{C}$ , and atmospheric pressure), the thermal properties of IRS-1 simulant, weighting 45 g, were analyzed at bulk density of  $1.97 \text{ g/cm}^3$ . The measured thermal conductivity, heat capacity, and thermal diffusivity are  $0.34 \pm 0.02 \text{ W/mK}$  ( $N = 3$ , 2SD),  $1.22 \pm 0.11 \text{ MJ/m}^3\text{K}$  ( $N = 3$ , 2SD), and  $0.28 \pm 0.04 \text{ mm}^2/\text{s}$  ( $N = 3$ , 2SD), respectively.

#### 4.8. Thermogravimetry

Thermal behaviour of regolith simulant is one of the factors to be considered in the application of simulant samples (e.g., 3D printing in space; Goulias et al., 2016). The mass changes of IRS-1 simulant and LL6 chondrite Sulagiri were recorded with Thermogravimetry (TG) experiments performed in standard atmosphere. The pattern for IRS-1 simulant is broadly consistent with that of the LL6 chondrite meteorite (Fig. 10). Both IRS-1 simulant and LL6 chondrite Sulagiri lost small ( $\sim 0.25$  wt% and  $\sim 0.02$  wt%, respectively) relative masses between 50 and  $\sim 500^\circ\text{C}$ . The released volatiles are most likely dominated by the H<sub>2</sub>O content and structure-H<sub>2</sub>O in these samples (Cannon et al., 2018). At  $\sim 500$ – $800^\circ\text{C}$ , the increase of relative mass in these two samples is most likely caused by the oxidation of ferrous (Fe<sup>2+</sup>) iron to ferric (Fe<sup>3+</sup>) iron in silicate minerals (e.g., olivine). At high temperature (i.e.,  $\sim 850$ – $900^\circ\text{C}$ ), both IRS-1 simulant and Sulagiri show a decrease of relative mass. Such observations may due to the release of SO<sub>2</sub> related to the thermal breakdown of troilite and pyrrhotite (Archer Jr. et al., 2018; Cannon et al., 2018).

**Table 4**

Bulk density and mechanical properties of the IRS-1 simulant and other prepared samples, compared with the asteroid regolith and simulants.

	Notes	Bulk density (g/cm <sup>3</sup> )	Cohesion (kPa) <sup>a</sup>	Angle of friction (°)	Reference
IRS-1	Itokawa/LL-chondrite-like	1.62	10.02	46.8 ± 0.37	This work
IRS-1L	L-chondrite-like	1.70	26.75	42.2 ± 0.12	This work
IRS-1H	H-chondrite-like	1.73	1.1	47.3 ± 0.35	This work
Asteroid regolith	Estimated value	1.0–2.2	0.1–5	15–40	Juaristi et al., 2015
Regolith simulant	For OSIRIS-REx mission	1.0–2.0	10 <sup>-4</sup> –10 <sup>3</sup>	15–47	Hergenrother et al., 2014
TLS simulant	Tagish Lake chondrite (C2)	1.0			Bierhaus et al., 2018
Itokawa blocks	From Hayabusa msission			40	Aoki et al., 2014
Itokawa asteroid	From Hayabusa msission	1.9 ± 0.13			Fujiwara et al., 2006

<sup>a</sup> The precise values of cohesion is difficult to determine because of the uncertainty of the intercept when the curved failure envelope is projected backwards to the  $\sigma_n = 0$  (Mitchell and Soga 1993; Monkul and Dacic 2017).

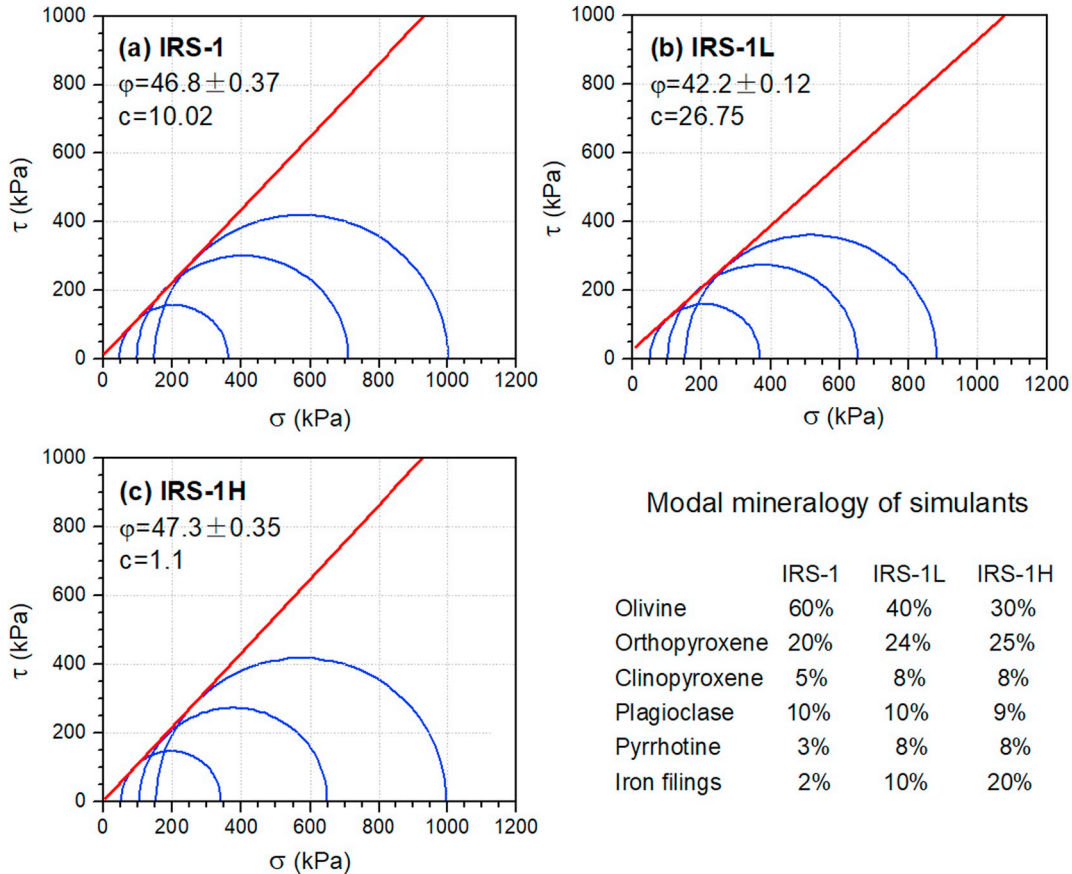


**Fig. 7.** The Mohr stress circles used to determine the angle of friction ( $\varphi$ ) and cohesion (c) for IRS-1 simulant (a), IRS-1L (b), and IRS-1H (c). The mineralogical components of IRS-1L and IRS-1H are similar to the L-chondrite and H-chondrite, respectively (see Table 1).

#### 4.9. Hygroscopic properties

The physical properties of simulants could vary by absorbing and/or adsorbing atmospheric water. To evaluate the hygroscopicity characteristics of IRS-1 simulant, this sample was placed in a drying cabinet (25 °C, 35% relative humidity) for 5 h and then placed in a tank at a temperature of 25 °C and a humidity of ~80%. Three samples, weighting 20 g respectively, were measured to obtain the hygroscopic properties of the IRS-1 simulant (see Fig. 11). The results show that moisture contents in IRS-1 simulant increased rapidly in the initial stage (i.e., within 1 h), and then reached a relatively stable value of ~2.2 wt% after 1.5 h (Fig. 11).

#### 5. Discussion

##### 5.1. The IRS-1 simulant compared to Itokawa samples and LL-chondrites

A combination of remote-sensing data, Itokawa sample, and chondrite meteorite (e.g., Sulagiri LL6) analyses have revealed that the S-type asteroids are composed primarily of silicates (> ~85%) with minor nickel-iron, troilite, and accessory minerals such as chromite and Ca-phosphate (e.g., Gaffey et al., 1993; Chapman, 1996; Nakamura et al., 2011; Tsuchiyama et al., 2014; Reddy et al., 2015). As for the composition of individual silicate phases of Itokawa samples and LL6 chondrite Sulagiri (Table 2; Nakamura et al., 2011), the olivine grains trend to be forsteritic olivine (~Fo<sub>75</sub>), pyroxene grains include pigeonite (~En<sub>75</sub>Wo<sub>1.4</sub>) and augite (~En<sub>46</sub>Wo<sub>45</sub>), and plagioclase tends to be albite (~Ab<sub>85</sub>). The IRS-1 simulant is, therefore, consistent with these findings as it is composed mostly (95%) of silicate minerals including

#### Modal mineralogy of simulants

	IRS-1	IRS-1L	IRS-1H
Olivine	60%	40%	30%
Orthopyroxene	20%	24%	25%
Clinopyroxene	5%	8%	8%
Plagioclase	10%	10%	9%
Pyrrhotite	3%	8%	8%
Iron filings	2%	10%	20%

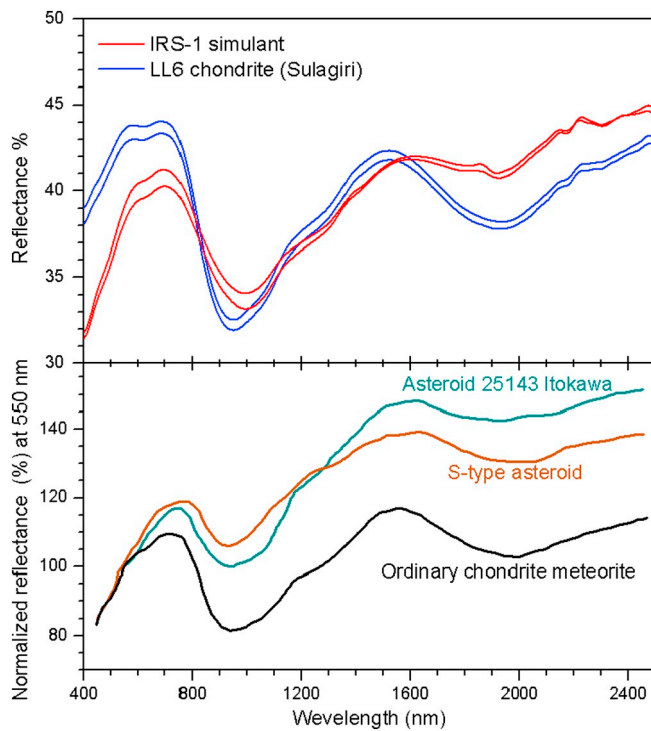


**Fig. 8.** Reflectance spectra of the IRS-1 simulant (red lines) and Sulagiri LL6 chondrite (blue lines) compared with Asteroid 25143 Itokawa, S-type asteroid, and ordinary chondrite meteorite (Binzel et al., 2001, 2010). (For interpretation of the references to colour in this figure legend, the reader is referred to the web version of this article.)

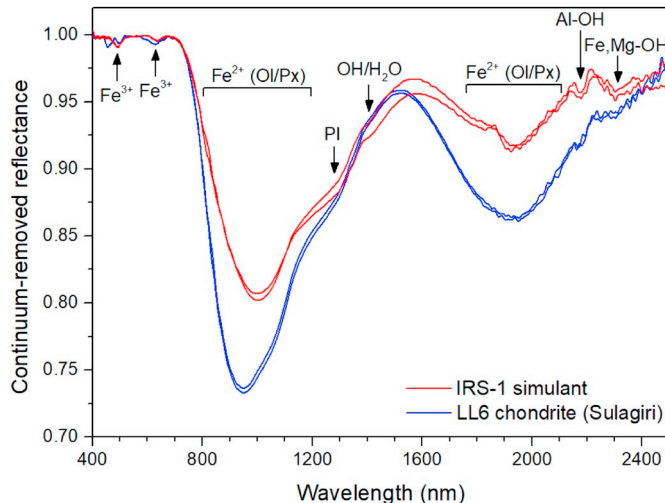


**Fig. 9.** Continuum removed spectra of IRS-1 (red lines) and Sulagiri LL6 chondrite (blue lines), showing the characteristic Fe<sup>3+</sup>, Fe<sup>2+</sup>, OH/H<sub>2</sub>O, and metal-OH absorptions present in these samples. (For interpretation of the references to colour in this figure legend, the reader is referred to the web version of this article.)

forsteritic olivine ( $\text{Fo}_{91.6}$ ), pigeonite ( $\text{En}_{69.3}\text{Wo}_{1.2}$ ), augite ( $\text{En}_{40.5}\text{Wo}_{44.8}$ ), and albite ( $\text{Ab}_{95.2}$ ) (Tables 1 and 2). However, it should be noted that the IRS-1 simulant does not contain nickel-iron and troilite that are rare on Earth, but these components were replaced with pyrrhotite and iron filings, respectively (Table 1). The lack of nickel-iron and troilite may affect the chemical composition (e.g., Ni) and spectral properties of this simulant.

Chemically, IRS-1 generally has a similar bulk composition as Itokawa samples and LL-chondrites, except for the iron ( $\text{FeO}/\text{Fe}_2\text{O}_3$ )

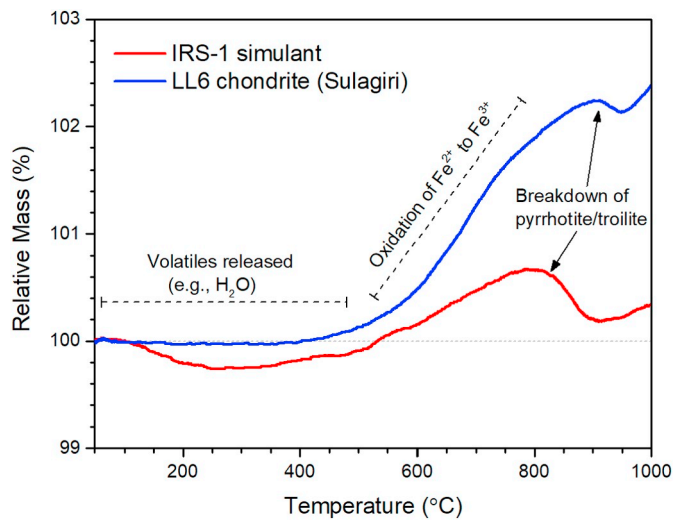


**Fig. 10.** Thermogravimetry of IRS-1 (red line) and LL6 chondrite Sulagiri (blue line) in atmospheric conditions. (For interpretation of the references to colour in this figure legend, the reader is referred to the web version of this article.)

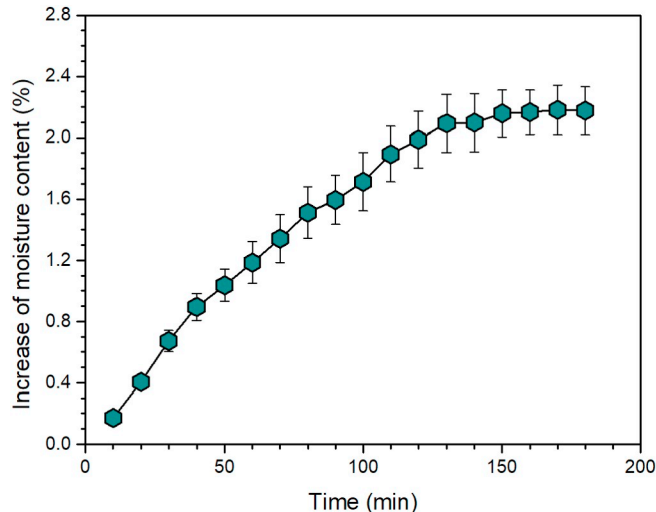


**Fig. 11.** Hygroscopic characteristics of the IRS-1 simulant.

and MgO abundance. Specifically, the Itokawa samples and LL-chondrites are composed of ~23–30 wt%  $\text{FeO}/\text{Fe}_2\text{O}_3$  and ~25–29 wt% MgO, respectively (Table 3). However, the IRS-1 simulant has a relatively low abundance of  $\text{Fe}_2\text{O}_3$  (15.8 wt%) and high abundance of MgO (34.3 wt%). This difference is most likely due to the fact that olivine grains ( $\text{Fo}_{91.6}$ ) in the IRS-1 simulant are more magnesium-rich than those in Itokawa samples and LL-chondrites ( $\text{Fo}_{-71-75}$ ) (Table 2). This interpretation is supported by the closely total iron and magnesium contents (i.e.,  $\text{FeO}/\text{Fe}_2\text{O}_3 + \text{MgO}$ ) of these samples (Table 3).

Measurements of IRS-1 show that this simulant is generally similar to LL6 Sulagiri chondrite with respect to spectral properties. Specifically, the absorption bands at ~1000 nm and ~2000 nm present in the spectrum of IRS-1 simulant are broadly similar to those in the measured Sulagiri LL6 chondrite (Fig. 8). However, absorptions at ~2200 and ~2300 nm caused by metal-OH are weaker in the spectrum of the Sulagiri chondrite than those in the spectrum of the IRS-1 simulant (Fig. 9). In addition, the spectral slopes present in spectra of the IRS-1 simulant are generally steeper than those of Sulagiri chondrite spectra (Fig. 8). This trend is consistent with the space weathering spectral trends (i.e., reddening of the asteroid spectra) observed in S-type asteroid spectra (Binzel et al., 2001, 2010; Clark et al., 2002).

The close-up images from the Hayabusa spacecraft have revealed that the Itokawa asteroid regolith is diverse in particle size, mostly ranging from sub-millimeter to centimeter scales (e.g., Fig. 1b; Yano et al., 2006; Miyamoto et al., 2007). However, the IRS-1 simulant is made up of sub-millimeter to millimeter particles (Fig. 5) which may not be consistent with the coarse-grained (i.e., millimeter to centimeter particles) Itokawa regolith grains. This difference in particle size may limit the potential applications of IRS-1 simulant, such as sample collection testing (e.g., Bierhaus et al., 2018).

Additionally, the grain density of IRS-1 simulant ( $3.37 \text{ g/cm}^3$ ) is close to the grain density for Itokawa particles ( $3.4 \text{ g/cm}^3$ ; Tsuchiyama et al., 2011) and also the LL-chondrite meteorites ( $3.54 \text{ g/cm}^3$ ; Consolmagno et al., 2008).

### 5.2. The limitations and potential improvements of IRS-1 simulant

The IRS-1 simulant is generally similar to S-type asteroid regolith with respect to mineralogy, bulk chemistry, reflectance spectra, and density (see discussions in Section 5.1). However, this simulant also has some drawbacks. For example: (1) Considering the different oxygen fugacities between terrestrial and asteroidal conditions during mineral formation, we note that the oxidation state of the iron likely differs between IRS-1 simulant and asteroid regolith; (2) S-type asteroids are mainly composed of ordinary chondrite-like materials, probably with a high abundance of rounded chondrules (Grady and Wright, 2006). However, the chondrules are absent in the IRS-1 simulant; (3) IRS-1 does not contain accessory minerals (e.g., phosphate and chromite) that are common in asteroid regoliths (Dunn et al., 2010); and (4) The  $< 2 \text{ mm}$  particle size of the IRS-1 simulant is not consistent with the coarse-grained (centimeter-sized or larger) materials on S-type asteroids.

Although it is challenging to produce regolith simulant exactly like the real asteroid regolith, there are many potential improvements for the preparation of IRS-1 simulant in the future: A series of simulants with different particle sizes (i.e., sub-millimeter to centimeter range) would be produced to expand the range of potential applications of simulants, such as sample collection testing. Also, other components (e.g., phosphate) should be considered as the additives for the development of future S-type asteroid regolith simulants.

### 5.3. Potential applications of IRS-1 simulant

Compared to the real asteroid materials (e.g., the spacecraft returned sample of Itokawa, and chondrite meteorites), IRS-1 has many advantages such as being low-cost to produce, having easy access to feedstock materials, and can be produced in large quantities. These characteristics make this simulant appropriate for use for a variety of applications where a large amount of sample is required. Because the physical properties (e.g., density and mechanical properties) of the IRS-1 simulant are in the range of asteroidal materials (Table 4), this sample was recommended for a wide range of geomechanical applications for asteroid exploration (Fig. 12). Such applications may include landing simulations, hardware testing, drilling, excavation, sampling technology development, verification testing, calibrating spectrometers, simulated landing of small spacecraft (e.g. CubeSats) onto asteroidal surfaces in a reduced-gravity environment, and mobility testing of systems such as microgravity rovers (e.g., Durda et al., 2013; Reid et al., 2014; Juaristi et al., 2015; Bierhaus et al., 2018; Fries et al., 2018). The absence of Fe–Ni metals in IRS-1 (Table 1) indicate that this simulant may have magnetic properties that are different from those of asteroid materials (e.g., ordinary chondrites; Consolmagno et al., 2008). We therefore can recommend using the IRS-1 simulant to test magnetism-related instrument. In addition, the relatively large specific density ( $3.37 \text{ g/cm}^3$ ) of IRS-1 suggests that this simulant is not suitable for representing low-weight asteroid regolith (e.g., Bierhaus et al., 2018).

IRS-1 has similar mineralogy to S-type asteroid material (Fig. 3 and

Applications	IRS-1
<b>Engineering-based testing</b>	
• Hardware and verification testing	●
• Sample collection tests	●
• Calibrating spectrometers	●
• Magnetism-related instrument testing	●
• Simulating low-weight regolith	⊗
• .....	
<b>Scientific experiments</b>	
• ISRU for asteroid materials	●
• 3D printing technologies development	●
• Spectra analysis of asteroids	⊗
• Geological investigation of asteroids	⊗
• .....	

● Recommended

○ Partially recommended

⊗ Not recommended

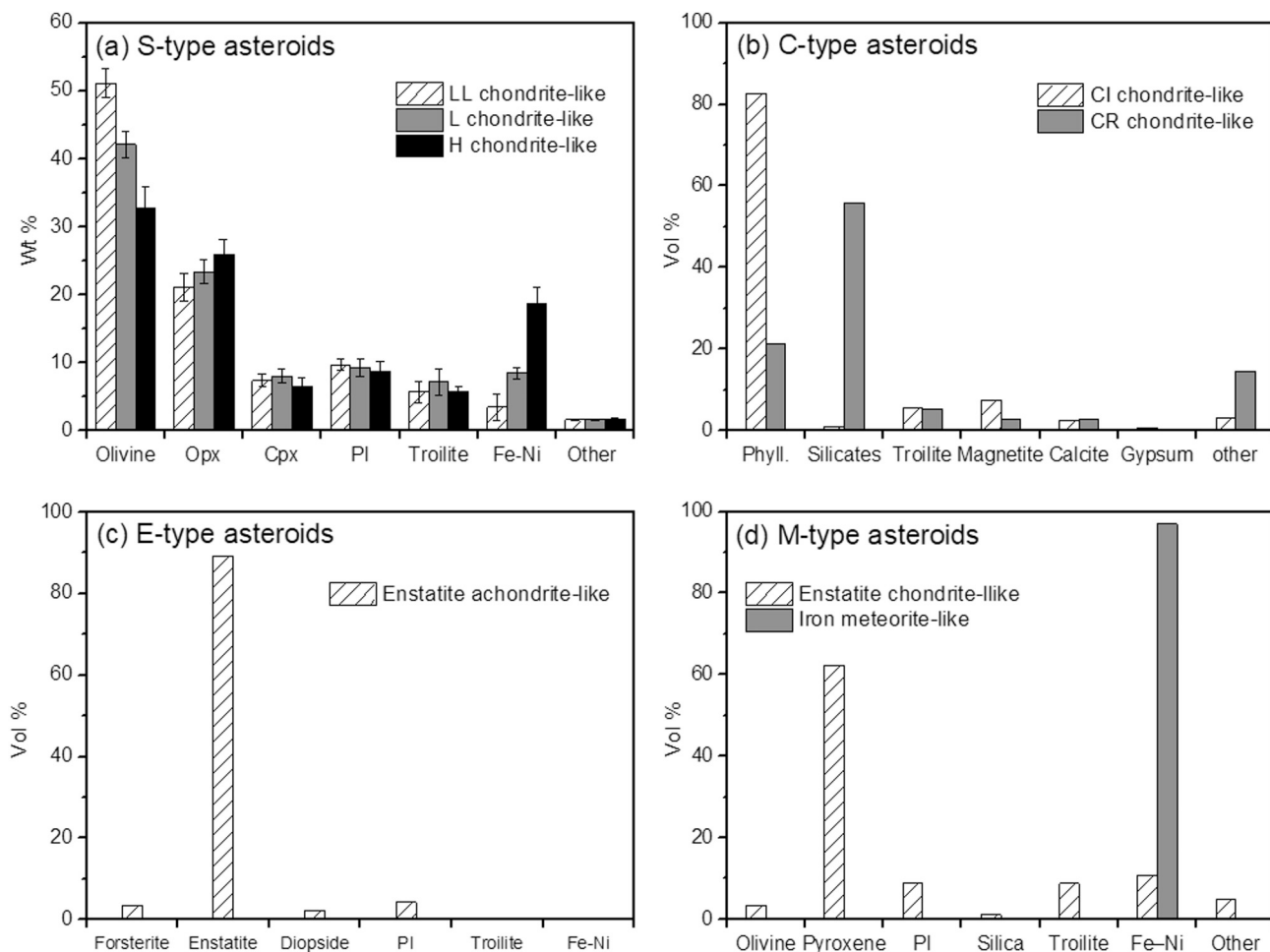
Fig. 12. Potential engineering and scientific applications of the IRS-1 simulant.

Table 1), so this simulant is recommended for large scale scientific experiments, including asteroid resources utilization testing (ISRU for asteroid materials), development of 3D printing technologies, and laboratory investigations of asteroid regolith properties (Fig. 12; Sanchez and McInnes, 2012; Durda et al., 2013; Feinman, 2013; Mazanek et al., 2015). However, for the laboratory studies that only require small amounts (i.e., a few grams to several hundred grams) of asteroid samples (e.g., for spectral analysis of asteroids and geological investigation of asteroids; Ford et al., 2008; Beck et al., 2010; Kohout et al., 2014), we do not recommend using the IRS-1 simulant. This is due to the difficulty of reproducing simulant material with consistent spectral and physical properties. In this case, small amounts of real asteroid materials (e.g., meteorites) would be a better choice because the fresh chondrite meteorites are easily accessible at a relatively low price (compared to lunar and/or Martian achondrites). For example, to experimentally investigate the partial melting processes of asteroids (e.g., Ford et al., 2008), chondrite meteorite samples are more reliable than small fractions of the IRS-1 simulant.

### 5.4. Effects of mineralogical variation on properties of S-type asteroid regoliths

The remote sensing and sample (e.g., Itokawa) investigations have shown that the S-type asteroid class is not mineralogically homogeneous (e.g., Gaffey et al., 1993; Tsuchiyama et al., 2011; Reddy et al., 2015). In particular, ordinary chondrite meteorite analysis revealed that this meteorite group (H, LL, and LL-chondrite) has relatively large mineralogical variations (Dunn et al., 2010): (1) The abundance of olivine varies from  $\sim 30 \text{ wt\%}$  in H-chondrites to  $\sim 60 \text{ wt\%}$  in LL-chondrites (Table 1); and (2) LL-chondrites have the least amount ( $\sim 3 \text{ wt\%}$ ) of FeNi metal, whereas H-chondrites contains the most (i.e.,  $\sim 20 \text{ wt\%}$ ). The mineralogical variation of ordinary chondrites suggests that the diverse S-type asteroid regoliths may have different physical and mechanical properties, which would be one of the critical considerations for asteroid exploration.

For IRS-1 and the other two prepared regolith simulant samples (i.e., L-chondrite-like IRS-1L and H-chondrite-like IRS-1H), mechanical property studies show that these samples have different angles of



**Fig. 13.** Mineralogical variations of different asteroid classes (i.e., S-type, C-type, E-type, and M-type) as told by meteorites. The average modal mineralogy of ordinary chondrites (LL, L, and H), carbonaceous chondrites (CI and CR), enstatite achondrites, and enstatite chondrites were taken from a range of literature (Dunn et al., 2010; Weisberg et al., 2009; Howard et al. 2010, 2015, King et al. 2015; Keil 2010). Opx = orthopyroxene; Cpx = clinopyroxene; Pl = plagioclase; Phyll. = phyllosilicate; Fe-Ni = Fe-Ni metal.

friction (Table 4), suggesting that the mineralogical variations on S-type asteroids have a relatively large influence on the mechanical properties of S-type asteroid regoliths. We therefore suggest that the mineralogical variations of regoliths could be an important consideration for asteroid landing and sampling activities in the future. For other properties, meteorite analyses have shown that the mineralogical variation of S-type asteroids would have relatively limited effects on the spectra of asteroid regolith (e.g., Vernazza et al., 2008; Flynn et al. 2017). However, the bulk chemistry (especially FeO content), magnetic properties, and thermal properties of asteroid materials can be largely affected by the mineralogical variation of S-type asteroid regoliths (especially by Fe–Ni metal that varies from ~3 wt% to 20 wt% in ordinary chondrites; Fig. 13a; Consolmagno et al., 2008; Flynn et al. 2017).

Although the surfaces of S-type asteroids are relatively heterogeneous in terms of mineralogy, our studies show that IRS-1 is generally a reasonable analogue of S-type asteroids and can be used in many applications. To meet the diverse mineralogy of S-type asteroids, the developed IRS-1 simulant would be used as the prototype asteroid regolith simulant. Other minerals can be added to this prototype simulant to develop a wide range of asteroid simulants with different mineral compositions like the IRS-1L and IRS-1H samples. For example, an E-type asteroid regolith simulant, which is dominated by enstatite minerals (Gaffey, 2002; Clark et al., 2004; Keller et al., 2010), can also be developed according to the mineralogy of E-type asteroids. These future versions of IRS-1 based simulants could be developed and used for

different objectives.

### 5.5. Implications for the development of asteroid regolith simulants

#### 5.5.1. Mineralogical variations of asteroid regoliths call for a wide range of simulants

Except for sample-return missions (e.g., Hayabusa spacecraft) and remote sensing observations (e.g., Dawn spacecraft), our knowledge about the mineralogy of asteroids can be extend by investigations of a variety of meteorites (Gaffey, 2002; Grady and Wright, 2006). Previous works have suggested that the S-type asteroids, C-type asteroids, E-type asteroids, and M-type asteroids are mineralogically similar to ordinary chondrites, carbonaceous chondrites (e.g., CI and CR), enstatite achondrites, and enstatite chondrites/iron meteorites, respectively (Gaffey and McCord, 1978; Rivkin, 2013). Modal mineralogy of these meteorite groups show that the regoliths on their parent-asteroid are highly heterogeneous among different asteroid classes (see Fig. 13). For example, (1) C-type asteroids commonly contain phyllosilicate phases formed following aqueous alteration (Hildebrand et al., 2006; Burbine et al., 2008; Howard et al., 2009). These components are nearly absent in other relatively dry asteroids, like the S-type asteroids (Gaffey et al. 2002); (2) E-type asteroids are dominated by enstatite minerals (over ~80 vol%; Fig. 13c); (3) some M-type asteroids are mainly composed of Fe–Ni metal, either pure or mixed with small amounts of stone (Fig. 13d); (4) Also, comets are icy bodies containing primitive materials with relatively high-porosity (e.g., Britt et al., 2006; Pätzold et al., 2013).

2016; Quirico et al., 2016).

Mineralogical variations of asteroids may lead to the properties of different asteroid regoliths being largely varied. Our studies demonstrate that the IRS-1 simulant is a reasonable surface analogue of S-type asteroids. However, this simulant is quite different from other types of asteroid regolith with respect to mineralogy and possibly to the mechanical properties (e.g., comet, C-type asteroid, and enstatite-rich E-type asteroid). The relatively large mineralogical variations of asteroid regoliths may call for a wide range regolith simulants for asteroid exploration applications, where IRS-1 could be used for many S-type asteroid regolith simulant applications.

### 5.5.2. Implications for the preparation of asteroid simulants

Most small asteroids (kilometer-sized or smaller) in the Solar System have not undergone magma differentiation and are mainly composed of primitive materials (e.g., like the chondrite meteorites). This indicates that the surfaces of small asteroids are not dominated by crystalline igneous rocks (e.g., basalts), which are common on differentiated bodies such as Mars, the Moon, and Vesta (Grady and Wright, 2006). Compared with the terrestrial crystallized basalts that have the compressive strength over ~200 MPa (Schultz, 1993), rocks on asteroids (especially C-type asteroids) are relatively brittle and have compressive strengths of less than ~100 MPa (Flynn et al. 2017). This indicates that terrestrial basalts may have physical properties largely different from the asteroid's surface materials, suggesting that terrestrial basalt may be not suitable as an asteroid surface analogue.

In many cases, planetary regolith simulants have been developed based on terrestrial volcanic glasses (e.g., CAS-1 lunar soil simulant and JSC Mars-1 Martian soil simulant; Allen et al., 1998; Zheng et al., 2009), terrestrial basalts (e.g., JMSS-1 martian soil simulant and Mojave mars simulant; Peters et al., 2008; Zeng et al., 2015), commercial sand products (e.g., ES-X Martian soil simulant; Gouache et al., 2011), and natural iron oxide deposits (e.g., SaltenSkov I mars dust simulant; Nørnberg et al., 2009). In addition, regolith simulants can be developed by mixing individual mineral phases, according to the designed mineral recipe (e.g., the MGS-1 Martian soil simulant and Y-Mars analogue; Cannon et al., 2018; Stevens et al., 2018). Similar to the MGS-1 and Y-Mars simulants, the IRS-1 simulant was developed via mixing of terrestrial mineral particles (Table 1). This study demonstrates that this mineral-mixing method has two advantages for the development of asteroid regolith simulants: (1) the multi-mineral mixing method is more flexible and effective to obtain a simulant with different mineral contents for different asteroid materials; (2) using this method, the mineral contents in simulants can be quantitatively designed for different applications. We therefore suggest that the studied approach for developing the IRS-1 simulant (i.e., mixing individual minerals) would be reliable for the development of other types of asteroid regolith (e.g., Comet, C-type asteroid, and enstatite-rich E-type asteroid) and potentially other planetary regolith simulants (e.g. for the Moon and Mars surface materials).

## 6. Conclusions

A new asteroid regolith simulant, IRS-1, has been developed from a combination of terrestrial minerals based on the mineralogy of Itokawa samples and LL-chondrites (e.g., Sulagiri LL6 chondrite meteorite). This simulant is a fine-grained (i.e., sub-millimeter to millimeter) powder that mainly consists of olivine, orthopyroxene, plagioclase, and clinopyroxene, with lesser amounts of pyrrhotite and iron filings. Our studies show that IRS-1 has similar mineralogy, bulk chemistry, reflectance spectra, and physical and mechanical properties to the target reference material (i.e., Itokawa samples and LL-chondrites), suggesting that IRS-1 is a reasonable representation of S-type asteroid regolith. However, this simulant also has some drawbacks, including the lack of Fe–Ni metal and accessory minerals (e.g., phosphate) observed in ordinary chondrites, the relatively Mg-rich olivine grains, and the absence

of centimeter-sized grains.

In this study, measurements of the mechanical properties of the IRS-1 simulant and two other prepared regolith simulants (i.e., the L-chondrite-like IRS-1 L and the H-chondrite-like IRS-1H) indicate that the mineralogical variations on S-type asteroids have a relatively large influence on the mechanical properties of S-type asteroid regolith. Compared with real asteroid materials such as chondrite meteorites, the IRS-1 simulant has many advantages (e.g., low-cost, easy access, and quantity production). This makes this simulant appropriate to be used for a variety of scientific and engineering applications where a large amount of sample is required, including asteroid resources utilization testing, hardware testing, drilling, excavation, and sampling technology development. In addition, the methodology adopted in this study can allow for the development of other types of regolith simulants (e.g., C-type and E-type) to meet a range of scientific and engineering requirements.

## Acknowledgments

This work was supported by the Strategic Priority Research Program (A) of Chinese Academy of Sciences (XDA15020000), National Natural Science Foundation of China (Grant Nos. 41490630, 41572037 and 41603066), Key Research Program of the Chinese Academy of Sciences (XDPB11), Youth Innovation Promotion Association of Chinese Academy of Sciences (2014359), and Beijing Municipal Science and Technology Commission (Z181100002918003). We thank Dr. Rosaly Lopes for the editorial handling and two anonymous reviewers for their constructive comments. We would like to thank Yangting Lin, Jianzong Liu, Yuyan Zhao, and Zhizhong Kang for their suggestions about the development of asteroid simulant. The authors would also like to thank Yong Meng, Shuqin Yang, Zhonghua Qin, Rui Li, Bing Mo, Ningbo Yao, and Ruilin Li for their help with the instrumental analyses. The IRS-1 simulant is available for other researchers and community and can be requested from Xiaojia Zeng ([zengxiaojia@mail.gyig.ac.cn](mailto:zengxiaojia@mail.gyig.ac.cn)) or Xiongyao Li ([lixiongyao@vip.skleg.cn](mailto:lixiongyao@vip.skleg.cn)).

## References

- Abe, M., Takagi, Y., Kitazato, K., Abe, S., Hiroi, T., Vilas, F., Clark, B.E., Abell, P.A., Lederer, S.M., Jarvis, K.S., Nimura, T., Ueda, Y., Fujiwara, A., 2006. Near-infrared spectral results of asteroid Itokawa from the Hayabusa spacecraft. *Science* 312 (5778), 1334–1338.
- Allen, C., Morris, R.V., Jager, K.M., Golden, D.C., Lindstrom, D.J., Lindstrom, M.M., Lockwood, J.P., 1998. Martian regolith simulant JSC Mars-1. In: Proceedings of the Lunar and Planetary Science Conference, XXIX, 29 Abstract #1690.
- Anbazhagan, S., Arivazhagan, S., 2009. Reflectance spectra of analog basalts; implications for remote sensing of lunar geology. *Planetary and Space Science* 57 (12), 1346–1358.
- Aoki, T., Nakamura, A., Hirata, N., 2014. Estimating the angle of friction of blocks on rubble-pile asteroid Itokawa. In: Asteroids, Comets, Meteors 2014.
- Archer Jr., P.D., Hogancamp, J.V., Gruener, J.E., Ming, D.W., 2018. Augmenting the Mojave Mars simulant to more closely match the volatile content of global Martian soils based on Mars science laboratory results. In: Proceedings of the Lunar and Planetary Science Conference, XLIX, 47 Abstract #2806.
- Beck, P., et al., 2010. Hydrous mineralogy of CM and CI chondrites from infrared spectroscopy and their relationship with low albedo asteroids. *Geochim. Cosmochim. Acta* 74, 4881–4892.
- Bierhaus, E.B., Clark, B.C., Harris, J.W., Payne, K.S., Dubisher, R.D., Wurts, D.W., Hund, R.A., Kuhns, R.M., Linn, T.M., Wood, J.L., May, A.J., Dworkin, J.P., Beshore, E., Lauretta, D.S., OSIRIS-REx Team, 2018. The OSIRIS-REx spacecraft and the Touch-and-Go Sample Acquisition Mechanism (TAGSAM). *Space Sci. Rev.* 214 (7), 107.
- Binzel, R.P., Rivkin, A.S., Bus, S.J., Sunshine, J.M., Burbine, T.H., 2001. MUSES-C target asteroid (25143) 1998 SF36: a reddened ordinary chondrite. *Meteorit. Planet. Sci.* 36, 1167–1172.
- Binzel, R.P., Morbidelli, A., Merouane, S., DeMeo, F.E., Birlan, M., Vernazza, P., Thomas, C.A., Rivkin, A.S., Bus, S.J., Tokunaga, A.T., Jan. 2010. Earth encounters as the origin of fresh surfaces on near-Earth asteroids. *Nature* 463, 331–334.
- Britt, D.T., 2015. Asteroid regolith simulants: development, characteristics, and testing. In: AGU Fall Meeting Abstracts, December.
- Britt, D.T., Consolmagno, S.J., Merline, W.J., 2006. Small Body Density and Porosity: New Data, New Insights. (LPSC XXXVII, 2214).
- Burbine, T.H., Rivkin, A.S., Noble, S.K., Monthe-Diniz, T., Bottke, W.F., McCoy, T.J., Dyar, M.D., Thomas, C.A., 2008. Oxygen and asteroids. *Rev. Mineral. Geochem.* 68, 273–343.

- Cannon, K.M., Britt, D.T., Smith, T.M., Fritsche, R.F., Batcheldor, D., 2019. Mars global simulant MGS-1: A Rocknest-based open standard for basaltic martian regolith simulants. *Icarus* 317, 470–478.
- Carey, E.M., Peters, G.H., Choukroun, M., Chu, L., Carpenter, E., Cohen, B., Panossian, L., Zhou, Y., Sarkissian, A., Moreland, S., Shiraishi, L.R., Backes, P., Zacny, K., Green, J.R., Raymond, C., 2017. Development and characteristics of mechanical porous ambient comet simulants as comet surface analogs. *Planetary and Space Science* 147, 6–13.
- Chapman, C.R., 1996. S-type asteroids, ordinary chondrites, and space weathering: the evidence from Galileo's fly-bys of Gaspra and Ida. *Meteorit. Planet. Sci.* 31 (6), 699–725.
- Clark, R., 1999. Spectroscopy of rocks and minerals, and principles of spectroscopy. *Manual Remote Sensing* 3, 3–58.
- Clark, B.E., Hapke, B., Pieters, C., Britt, D., 2002. Asteroid space weathering and regolith evolution. In: *Asteroids III*. vol. 585.
- Clark, B.E., Bus, S.J., Rivkin, A.S., McConnochie, T., Sanders, J., Shah, S., Shepard, M., 2004. E-type asteroid spectroscopy and compositional modeling. *Journal of Geophysical Research: Planets* 109 (E2).
- Consolmagno, G., Britt, D., Macke, R., 2008. The significance of meteorite density and porosity. *Chem. Erde* 68, 1–29. <https://doi.org/10.1016/j.chemer.2008.01.003>.
- Covey, S.D., Lewis, J.S., Metzger, P.T., Britt, D.T., 2018. Developing carbonaceous chondrite asteroid simulants. In: *Earth and Space*. vol. 8.
- Delbo, M., Libourel, G., Wilkerson, J., Murdoch, N., Michel, P., Ramesh, K.T., Ganino, C., Verati, C., Marchi, S., 2014. Thermal fatigue as the origin of regolith on small asteroids. *Nature* 508 (7495), 233.
- Deng, Y.F., Song, X.Y., Hollings, P., Chen, L.M., Zhou, T., Yuan, F., Xie, W., Zhang, D., Zhao, B., 2017. Lithological and geochemical constraints on the magma conduit systems of the Huangshan Ni-Cu sulfide deposit, NW China. *Mineral. Deposita* 52 (6), 845–862.
- Dreyer, C.B., Abdal-Madrid, A., Atkinson, J., Lampe, A., Markley, T., Williams, H., McDonough, K., Canney, T., Haines, J., 2018. A new experimental capability for the study of regolith surface physical properties to support science, space exploration, and in situ resource utilization (ISRU). *Rev. Sci. Instrum.* 89 (6), 064502.
- Dunn, T.L., Cresssey, G., McSweeney Jr., H.Y., McCoy, T.J., 2010. Analysis of ordinary chondrites using powder X-ray diffraction: 1. Modal mineral abundances. *Meteorit. Planet. Sci.* 45, 123–134. <https://doi.org/10.1111/j.1945-5100.2009.01011.x>.
- Durda, D., Devaud, G., Scheeres, D., Sánchez, P., Roark, S., Kapchen, P., ... Bagatin, A.C., 2013. Laboratory investigation of asteroid regolith properties. *EPSC 2013 Proceedings*.
- Durda, D., Devaud, G., Scheeres, D., Sánchez, P., Roark, S., Kapchen, P., ... Campo Bagatin, A., 2013. Laboratory investigation of asteroid regolith properties. In: *EPSC 2013 Proceedings*.
- Feinman, M., 2013. Mining the final frontier: keeping Earth's asteroid mining ventures from becoming the next gold rush. *Pitt. J. Tech. L. & Pol'y* 14, 202.
- Ford, R.L., Benedix, G.K., McCoy, T.J., Rushmer, T., 2008. Partial melting of H6 ordinary chondrite Kernouvé: constraints on the effects of reducing conditions on oxidized compositions. *Meteorit. Planet. Sci.* 43 (8), 1399–1414.
- Fries, M., Abell, P., Brisset, J., Britt, D., Colwell, J., Dove, A., Durda, D., Graham, L., Hartzell, C., Hrovat, K., John, K., Karrer, D., Leonard, M., Love, S., Morgan, J., Poppin, J., Rodriguez, V., Sanchez-Lana, P., Scheeres, D., Whizin, A., 2018. The Strata-1 experiment on small body regolith segregation. *Acta Astronautica* 142, 87–94.
- Fujiwara, A., Kawaguchi, J., Yeomans, D.K., Abe, M., Mukai, T., Okada, T., et al., 2006. The rubble-pile asteroid Itokawa as observed by Hayabusa. *Science* 312 (5778), 1330–1334.
- Flynn, G.J., Consolmagno, G.J., Brown, P., Macke, R.J., 2017. Physical properties of the stone meteorites: Implications for the properties of their parent bodies. *Chemie der Erde*.
- Gaffey, M.J., 2002. Mineralogy of asteroids. In: *AIP Conference Proceedings*. vol. 1386, No. 1. AIP, pp. 129–169.
- Gaffey, M.J., McCord, T.B., 1978. Asteroid surface materials: mineralogical characterizations from reflectance spectra. *Space Sci. Rev.* 21 (5), 555–628.
- Gaffey, M.J., Bell, J.F., Brown, R.H., Burbine, T.H., Piatek, J.L., Reed, K.L., Chaky, D.A., 1993. Mineralogical variations within the S-type asteroid class. *Icarus* 106 (2), 573–602.
- Gouache, T.P., Patel, N., Brunskill, C., Scott, G.P., Saaj, C.M., Matthews, M., Cui, L., 2011. Soil simulant sourcing for the ExoMars rover testbed. *Planet. Space Sci.* 59, 779–787. <https://doi.org/10.1016/j.pss.2011.03.006>.
- Goulas, A., Engstrom, D.S., Friel, R.J., Harris, R.A., 2016. Investigating the Additive Manufacture of Extra-Terrestrial Materials.
- Grady, M.M., Wright, I., 2006. Types of extraterrestrial material available for study. In: *Meteorites and the Early Solar System II*. University of Arizona Press, Tucson, pp. 3–18.
- Gundlach, B., Blum, J., 2013. A new method to determine the grain size of planetary regolith. *Icarus* 223 (1), 479–492.
- Hergenrother, C.W., et al., 2014. The design reference asteroid for the OSIRIS-Rex Mission Target (101955) Bennu. <http://arxiv.org/abs/1409.4704>.
- Hildebrand, A.R., McCausland, P.J.A., Brown, P.G., Longstaffe, F.J., Russell, S.D.J., Tagliaferri, E., Wacker, J.F., Mazur, M.J., 2006. The fall and recovery of the Tagish Lake meteorite. *Meteorit. Planet. Sci.* 41, 407–431.
- Hildebrand, A.R., Hanton, L.T.J., Rankin, M., Ibrahim, M.I., 2015, July. An asteroid regolith simulant for Hydrated Carbonaceous Chondrite Lithologies (HCCL-1). In: *78th Annual Meeting of the Meteoritical Society*. vol. 1856. pp. 5368.
- Howard, K.T., Benedix, G.K., Bland, P.A., Cressey, G., 2009. Modal mineralogy of CM2 chondrites by X-ray diffraction (PSD-XRD). Part 1: total phyllosilicate abundance and the degree of aqueous alteration. *Geochim. Cosmochim. Acta* 73 (15), 4576–4589.
- Howard, K.T., Benedix, G.K., Bland, P.A., Cressey, G., 2010. Modal mineralogy of CV3 chondrites by X-ray diffraction (PSD-XRD). *Geochimica et Cosmochimica Acta* 74 (17), 5084–5097.
- Jarosewich, E., 1990. Chemical analyses of meteorites: a compilation of stony and iron meteorite analyses. *Meteoritics* 25 (4), 323–337.
- Jewitt, D., Weaver, H., Agarwal, J., Mutchler, M., Drahus, M., 2010. A recent disruption of the main-belt asteroid P/2010A2. *Nature* 467, 817–819.
- Juaristi, C.O., Martínez, E.O., Astigarraga, M.C., Etxaniz, X.A., Martínez-Frías, J., Romstedt, J., Le Letty, R., 2015. Development and Ground Test Campaign of a Sampling Tool Mechanism for Low Gravity Bodies. *Astra*.
- Keil, K., 2010. Enstatite achondrite meteorites (aubrites) and the histories of their asteroidal parent bodies. *Chemie der Erde-Geochemistry* 70 (4), 295–317.
- Keller, L.P., Berger, E.L., 2014. A transmission electron microscope study of Itokawa regolith grains. *Earth, Planets and Space* 66, 1–7.
- Keller, H.U., Barbieri, C., Koschny, D., Lamy, P., Rickman, H., Rodrigo, R., Siersks, H., A'Hearn, M.F., Angrilli, F., Barucci, M.A., Bertaux, J.-L., Cremonese, G., Da Deppo, V., Davidsson, B., De Cecco, M., Debei, S., Fornasier, S., Fulle, M., Groussin, O., Gutierrez, P.J., Hviid, S.F., Ip, W.-H., Jorda, L., Knollenberg, J., Kramm, J.R., Küht, E., Küppers, M., Lara, L.-M., Lazzarin, M., Moreno, J.L., Marzari, F., Michalik, H., Naletto, G., Sabau, L., Thomas, N., Wenzel, K.-P., Bertini, I., Besse, S., Ferri, F., Kaasalainen, M., Lowry, S., Marchi, S., Mottola, S., Sabolo, W., Schröder, S.E., Spjuth, S., Vernazza, P., 2010. E-type asteroid (2867) steins as imaged by OSIRIS on Board Rosetta. *Science* 327, 190–193.
- King, A.J., Schofield, P.F., Howard, K.T., Russell, S.S., 2015. Modal mineralogy of CI and CI-like chondrites by X-ray diffraction. *Geochimica et Cosmochimica Acta* 165, 148–160.
- Kohout, T., Gritsevich, M., Grokhovsky, V.I., Yakovlev, G.A., Haloda, J., Halodova, P., Muinonen, K., 2014. Mineralogy, reflectance spectra, and physical properties of the Chelyabinsk LL5 chondrite—insight into shock-induced changes in asteroid regoliths. *Icarus* 228, 78–85.
- Langenhorst, F., Harries, D., Pollock, K., van Aken, P.A., 2014. Mineralogy and defect microstructure of an olivine-dominated Itokawa dust particle: evidence for shock metamorphism, collisional fragmentation, and LL chondrite origin. *Earth, Planets and Space* 66 (1), 118.
- Li, C., Liu, J., Ren, X., Zuo, W., Tan, X., Wen, W., Li, H., Mu, L., Su, Y., Zhang, H., Yan, J., Ouyang, Z., 2015. The Chang'e 3 mission overview. *Space Sci. Rev.* 190 (1–4), 85–101.
- Li, R., Zhou, G., Hall, M.R., 2018. Arching effect of planetary regolith simulant under extraterrestrial gravities. *J. Aerosp. Eng.* 31 (6).
- Matsumoto, T., Tsuchiyama, A., Uesugi, K., Nakano, T., Uesugi, M., Matsuno, J., Nagano, T., Shimada, A., Takeuchi, A., Suzuki, Y., Nakamura, T., Nakamura, M., Gucsis, A., Nagaki, K., Sakaiya, T., Kondo, T., 2016. Nanomorphology of Itokawa regolith particles: application to space-weathering processes affecting the Itokawa asteroid. *Geochim. Cosmochim. Acta* 187, 195–217.
- Matsumoto, T., Hasegawa, S., Nakao, S., Sakai, M., Yurimoto, H., 2018. Population characteristics of submicrometer-sized craters on regolith particles from asteroid Itokawa. *Icarus* 303, 22–33.
- Mazanek, D.D., Merrill, R.G., Brophy, J.R., Mueller, R.P., 2015. Asteroid redirect mission concept: a bold approach for utilizing space resources. *Acta Astronautica* 117, 163–171.
- Meng, Y., Gong, G., Wei, D., Xie, Y., 2016. In situ high temperature X-ray diffraction study on high strength aluminous porcelain insulator with the Al<sub>2</sub>O<sub>3</sub>-SiO<sub>2</sub>-K<sub>2</sub>O-Na<sub>2</sub>O system. *Appl. Clay Sci.* 132, 760–767.
- Miyamoto, H., Yano, H., Scheeres, D.J., Abe, S., Barnouin-Jha, O., Cheng, A.F., Demura, H., Gaskell, R., Hirata, N., Ishiguro, M., Michikami, T., Nakamura, A., Nakamura, R., Saito, J., Sasaki, S., 2007. Regolith migration and sorting on asteroid Itokawa. *Science* 316 (5827), 1011–1014.
- Mitchell, J.K., Soga, K., 1993. Fundamentals of Soil Behavior. 422 John Wiley & Sons. Inc., New York.
- Monkul, M.M., Dacic, A., 2017. Effect of grain size distribution on stress-strain behavior of lunar soil simulants. *Advances in Space Research* 60 (3), 636–651.
- Nakamura, T., Noguchi, T., Tanaka, M., Zolensky, M.E., Kimura, M., Tsuchiyama, A., Nakato, A., Ogami, T., Ishida, H., Uesugi, M., Yada, T., Shirai, K., Fujimura, A., Okazaki, R., Sandford, S.A., Ishibashi, Y., Abe, M., Okada, T., Ueno, M., Mukai, T., Yoshikawa, M., Kawaguchi, J., 2011. Itokawa dust particles: a direct link between S-type asteroids and ordinary chondrites. *Science* 333, 1113–1116.
- Nakamura, T., et al., 2014. Mineral chemistry of MUSES-C Regio inferred from analysis of dust particles collected from the first- and second touchdown sites on asteroid Itokawa. *Meteorit. Planet. Sci.* 49, 215–227.
- Nørnberg, P., Gunnlaugsson, H.P., Merrison, J.P., Vendelboe, A.L., 2009. Salten Skov 1: a Martian magnetic dust analogue. *Planet. Space Sci.* 57, 628–631. <https://doi.org/10.1016/j.pss.2008.08.017>.
- Noviello, J.L., Ernst, C.M., Barnouin, O.S., Daly, M., 2014. Block distribution on Itokawa: implications for asteroid surface evolution. In: *Lunar and Planetary Science Conference*. vol. 45. pp. 1587.
- Ouyang, Z., Li, C., Zou, Y., Zhang, H., Lü, C., Liu, J., Liu, J., Zuo, W., Su, Y., Wen, W., Bian, W., Zhao, B., Wang, J., Yang, J., Chang, J., Wang, H., Zhang, X., Wang, S., Wang, M., Ren, X., Mu, L., Kong, D., Wang, X., Wang, F., GENG, L., Zhang, Z., Zheng, L., Zhu, X., Zheng, Y., Li, J., Zou, X., Xu, C., Shi, S., Gao, Y., Gao, G., 2010. Primary scientific results of Chang'E-1 lunar mission. *Science China Earth Sciences* 53 (11), 1565–1581.
- Pätzold, M., Anderl, T., Hahn, M., Asmar, S.W., Barriot, J.P., Bird, M.K., Häusler, B., Peter, K., Tellmann, S., Grüni, E., Weissman, P.R., 2016. A homogeneous nucleus for comet 67P/Churyumov-Gerasimenko from its gravity field. *Nature* 530 (7588), 63–65 (Prialnik, D., Podolak, J.).
- Peters, G.H., Abbey, W., Bearman, G.H., Mungas, G.S., Smith, J.A., Anderson, R.C., Douglas, S., Beegle, L.W., 2008. Mojave Mars simulant – characterization of a new

- geologic Mars analog. *Icarus* 197, 470–479.
- Qin, Z., Wan, Q., Li, S., Fu, Y., Gu, Y., Yang, S., Zhang, J., 2017. TGA-FTIR study of the pyrolysis and combustion of montmorillonite-tobacco mixtures. *J. Nanosci. Nanotechnol.* 17 (9), 6423–6432.
- Quirico, E., Moroz, L.V., Schmitt, B., Arnold, G., Faure, M., Beck, P., Bonal, L., Ciarniello, M., Capaccioni, F., Filacchione, G., Erard, S., 2016. Refractory and semivolatile organics at the surface of comet 67P/Churyumov-Gerasimenko: insights from the VIRTIS/Rosetta imaging spectrometer. *Icarus* 272, 32–47.
- Reddy, V., Sanchez, J.A., Bottke, W.F., Cloutis, E.A., Izawa, M.R.M., O'Brien, D.P., Mann, P., Cuddy, M., Le Corre, L., Gaffey, M.J., Fujihara, G., 2014. Chelyabinsk meteorite explains unusual spectral properties of Baptista asteroid family. *Icarus* 237, 116–130.
- Reddy, V., Dunn, T.L., Thomas, C.A., Moskovitz, N.A., Burbine, T.H., 2015. Mineralogy and surface composition of asteroids. In: *Asteroids IV*. University of Arizona Press, Tucson, AZ, pp. 43–64.
- Reid, R.G., Roveda, L., Nesnas, I.A., Pavone, M., 2014. Contact Dynamics of Internally-actuated Platforms for the Exploration of Small Solar System Bodies. In: *Proceedings of I-SAIRAS*.
- Rivkin, A., 2013. An overview of the asteroids and meteorites. *Planets Stars & Stellar Systems* 376–429.
- Rubin, A.E., Ma, C., 2017. Meteoritic minerals and their origins. In: *Chemie der Erde-Geochimistry*.
- Sakatani, N., Ogawa, K., Arakawa, M., Tanaka, S., 2018. Thermal conductivity of lunar regolith simulant JSC-1A under vacuum. *Icarus* 309, 13–24.
- Sanchez, J.P., McInnes, C.R., 2012. Assessment on the feasibility of future shepherding of asteroid resources. *Acta Astronautica* 73, 49–66.
- Sánchez, P., Scheeres, D.J., 2014. The strength of regolith and rubble pile asteroids. *Meteorit. Planet. Sci.* 49 (5), 788–811.
- Scheeres, D.J., Hartzell, C.M., Sánchez, P., Swift, M., 2010. Scaling forces to asteroid surfaces: the role of cohesion. *Icarus* 210 (2), 968–984.
- Schlutz, R.A., 1993. Brittle strength of basaltic rock masses with applications to Venus. *Journal of Geophysical Research: Planets* 98 (E6), 10883–10895.
- Seiferlin, K., Ehrenfreund, P., Garry, J., Gunderson, K., Hütter, E., Kargl, G., Maturilli, A., Merrison, J.P., 2008. Simulating Martian regolith in the laboratory. *Planetary and Space Science* 56, 2009–2025. <https://doi.org/10.1016/j.pss.2008.09.01>.
- Siegler, M., Aharonson, O., Carey, E., Choukroun, M., Hudson, T., Schorghofer, N., Xu, S., 2012. Measurements of thermal properties of icy Mars regolith analogs. *Journal of Geophysical Research: Planets* 117 (E3).
- Stevens, A.H., Steer, E., McDonald, A., Amador, E.S., Cockell, C.S., 2018. Y-Mars: an astrobiological analogue of martian mudstone. *Earth and Space Science* 5 (4), 163–174.
- Street Jr., K.W., Ray, C., Rickman, D., Scheiman, D.A., 2010. Thermal properties of lunar regolith simulants. In: *Earth and Space 2010: Engineering, Science, Construction, and Operations in Challenging Environments*, pp. 266–275.
- Thuillet, F., Michel, P., Maurel, C., Ballouz, R.L., Zhang, Y., Richardson, D.C., Biele, J., Tatsumi, E., Sugita, S., 2018. Numerical modeling of lander interaction with a low-gravity asteroid regolith surface—application to MASCOT on board Hayabusa2.
- Astronomy & Astrophysics 615, A41.
- Tsuchiyama, A., Uesugi, M., Matsushima, T., Michikami, T., Kadono, T., Nakamura, T., Uesugi, K., Nakano, T., Sandford, S.A., Noguchi, R., Matsumoto, T., Matsuno, J., Nagano, T., Imai, Y., Takeuchi, A., Suzuki, Y., Ogami, T., Katagiri, J., Ebihara, M., Ireland, T.R., Kitajima, F., Nagao, K., Naraoka, H., Noguchi, T., Okazaki, R., Yurimoto, H., Zolensky, M.E., Mukai, T., Abe, M., Yada, T., Fujimura, A., Yoshikawa, M., Kawaguchi, J., 2011. Three-dimensional structure of Hayabusa samples: origin and evolution of Itokawa regolith. *Science* 333, 1125–1128.
- Tsuchiyama, A., Uesugi, M., Uesugi, K., Nakano, T., Noguchi, R., Matsumoto, T., Matsuno, J., Nagano, T., Imai, Y., Shimada, A., Takeuchi, A., Suzuki, Y., Nakamura, T., Noguchi, T., Abe, M., Yada, T., Fujimura, A., 2014. Three-dimensional microstructure of samples recovered from asteroid 25143 Itokawa: comparison with LL5 and LL6 chondrite particles. *Meteorit. Planet. Sci.* 49, 172–187.
- Vernazza, P., Binzel, R.P., Thomas, C.A., DeMeo, F.E., Bus, S.J., Rivkin, A.S., Tokunaga, A.T., 2008. Compositional differences between meteorites and near-Earth asteroids. *Nature* 454 (7206), 858.
- Wei, Y., Yao, Z., Wan, W., 2018. China's roadmap for planetary exploration. *Nature Astronomy* 2 (5), 346.
- Weisberg, M.K., Smith, C., Benedix, G., Herd, C.D., Righter, K., Haack, H., Yamaguchi, A., Chennaoui Aoudjehane, H., Grossman, J.N., 2009. The meteoritical bulletin, no. 96, September 2009. *Meteorit. Planet. Sci.* 44 (9), 1355–1397.
- Whitney, D.L., Evans, B.W., 2010. Abbreviations for names of rock-forming minerals. *Am. Mineral.* 95 (1), 185–187.
- Yamada, T.M., Ando, K., Morota, T., Katsuragi, H., 2016. Timescale of asteroid resurfacing by regolith convection resulting from the impact-induced global seismic shaking. *Icarus* 272, 165–177.
- Yano, H., Kubota, T., Miyamoto, H., Okada, T., Scheeres, D., Takagi, Y., Yoshida, K., Abe, M., Abe, S., Barnouin-Jha, O., Fujiwara, A., Hasegawa, S., Hashimoto, T., Ishiguro, M., Kato, M., Kawaguchi, J., Mukai, T., Saito, J., Sasaki, S., Yoshikawa, M., 2006. Touchdown of the Hayabusa spacecraft at the Muses Sea on Itokawa. *Science* 312 (5778), 1350–1353.
- Yu, W., Li, X., Wang, S., 2016. Laboratory thermal conductivity measurement of pyroxene powder under low temperature and atmospheric pressure conditions: implication for the studies on lunar and Martian surface thermal environment. *Acta Petrol. Sin.* 32 (1), 99–106.
- Zeng, X., Li, X., Wang, S., Li, S., Spring, S., Tang, H., Li, Y., Feng, J., 2015. JMSS-1: a new Martian soil simulant. *Earth Planets Space* 67. <https://doi.org/10.1186/s40623-015-0248-5>.
- Zeng, X., Joy, K.H., Li, S., Pernet-Fisher, J.F., Li, X., Martin, D.J., Li, Y., Wang, S., 2018. Multiple lithic clasts in lunar breccia Northwest Africa 7948 and implication for the lithologic components of lunar crust. *Meteorit. Planet. Sci.* 53 (5), 1030–1050.
- Zhang, T., Zhang, W., Wang, K., Gao, S., Hou, L., Ji, J., Ding, X., 2017. Drilling, sampling, and sample-handling system for China's asteroid exploration mission. *Acta Astronautica* 137, 192–204.
- Zheng, Y., Wang, S., Ouyang, Z., Zou, Y., Liu, J., Li, C., Li, X., Feng, J., 2009. CAS-1 lunar soil simulant. *Adv. Space Res.* 43, 448–454.